

ENabling Optimized DISruptivE airframe-propulsion integration concepts

H2020 Research and Innovation Action
Grant Agreement No 860103

Deliverable Reference Number: D3.6

Deliverable Title:
Documentation of experimental databases (without mitigation)

Lead participant: NLR
Contributing participant(s): UBRI, UTWE, TUD, ECL, VKI

September 13, 2023

Start date of project: 1st of June 2020
Duration: 48 months
Due date of deliverable: T0 + 11 = 31 August 2023

Type		
R	Document, report	X
DEM	Demonstrator, pilot, prototype, etc.	
DEC	Websites, patent fillings, videos, etc.	
ORDP	Open Research Data Pilot	
Dissemination Level		
PU	Public	X
CO	Confidential, only for members of the consortium (incl. Commission Services)	

APPROVAL

Title	Issue	Revision
Documentation of experimental databases (without mitigation)	1	0

Author(s)	Date
H. Dekker (TUD/NLR), I. Zaman (UBRI), F. do Nascimento Monteiro (TUD), D. Acevedoci (ECL), M. Roger (ECL), E. Gallo (VKI)	11/09/2023

Approved by	Date
C. Schram (VKI)	13/09/2023

Contents

1 Introduction **5**

2 A1 - UTWE **5**
2.1 Aeroacoustics Facility . . . 5
2.1.1 University of Twente Wind Tunnel . . . 5
2.1.2 Far-field acoustic microphone arrays . . . 5
2.1.3 Hotwire Anemometry . . . 5
2.1.4 Near-field instrumentation . . . 5
2.1.5 Performance and RIG instrumentation . . . 5
2.2 A1 Experimental Campaign UTWE . . . 6
2.2.1 Overview . . . 6
2.2.2 Boundary Layer . . . 7
2.2.3 Instrumented flat plate . . . 7
2.2.4 Test matrix . . . 7
2.2.5 Database structure . . . 8
2.2.6 A1 CAD Geometry Database . . . 9

3 A - UBRI **9**
3.1 Aeroacoustic Facility . . . 9
3.1.1 Anechoic chamber and wind tunnel . . . 9
3.1.2 Far-field acoustic microphone arrays . . . 9
3.1.3 Hotwire Anemometry . . . 10
3.1.4 Near-field Instrumentation . . . 10
3.1.5 Propeller Rig . . . 10
3.1.6 Control and Data Acquisition System . . . 11
3.2 A1 - UBRI . . . 12
3.2.1 Overview . . . 12
3.2.2 Flat Plate Instrumentation Distribution . . . 12
3.2.3 Test Matrix . . . 13
3.2.4 Database structure . . . 15
3.2.5 A1 CAD Geometry Database . . . 15
3.3 A2 - UBRI . . . 15
3.3.1 Overview and Schematic . . . 15
3.3.2 S-Plate Instrumentation Distribution . . . 16
3.3.3 Test Matrix . . . 17
3.3.4 Database structure . . . 18
3.3.5 A2 CAD Geometry Database . . . 19

4 B1 - TUD **19**
4.1 Wind Tunnel Facility . . . 19
4.2 Experimental Setup . . . 20
4.3 Test Conditions and Configurations . . . 20
4.4 Measurement Techniques . . . 21
4.5 Data Availability . . . 23

5 B2-ECL **23**
5.1 Setup Description . . . 23
5.2 Dimensional Considerations . . . 24
5.3 Wind Tunnel Facility . . . 27
5.4 Test Conditions . . . 27
5.4.1 Numerical Simulations . . . 27
5.4.2 Selected Reference Configuration . . . 28
5.5 Instrumentation . . . 28
5.5.1 Acoustic Measurements . . . 28
5.5.2 Static Pressure Measurements . . . 29
5.5.3 Aerodynamic Forces Measurements . . . 30
5.6 Data availability . . . 30

6 B3-VTOL **30**
6.1 Wind Tunnel facility . . . 30
6.2 Propeller model . . . 30
6.3 Operating conditions . . . 30
6.4 Measurement Techniques . . . 31
6.4.1 Lagrangian Particle Tracking . . . 31
6.4.2 TR-PIV . . . 33
6.5 Data availability & naming conventions . . . 34

7 B3-Flap **34**
7.1 Wind Tunnel facility . . . 34
7.2 Propeller and wing model . . . 35
7.3 Operating conditions . . . 35
7.3.1 Isolated propeller . . . 35
7.3.2 Single propeller over-the-wing . . . 36
7.3.3 Distributed propellers over-the-wing . . . 36
7.4 Measurement Techniques . . . 36
7.4.1 Integral loading . . . 36
7.4.2 Acoustics . . . 37
7.4.3 Pressure orifices . . . 37
7.4.4 Stereoscopic Particle Image Velocimetry . . . 37
7.4.5 2C Particle Image Velocimetry . . . 38
7.5 Data availability & naming conventions . . . 38

8 C - VKI **39**
8.1 Description of the ALCOVES anechoic test room . . . 39
8.1.1 Design of the coaxial rotors system and instrumentation structure . . . 39
8.1.2 Acoustic . . . 42
8.1.3 Content of the dataset . . . 43

9 Conclusions **45**

1 Introduction

This deliverable concerns all the necessary documentation of the experimental databases which have been shared in the deliverables D3.3, D3.4 and D3.5. The documentation consists of a description of the wind tunnel facilities, wind tunnel model (incl. CAD files), operating conditions, measurement techniques and data availability (incl. file naming conventions). Each of the configurations investigated within WP3 will be treated separately.

2 A1 - UTWE

2.1 Aeroacoustics Facility

2.1.1 University of Twente Wind Tunnel

The A1 experiments were executed in the University of Twente acoustic wind tunnel. The facility consists of a $6 \times 6 \times 4$ m^3 anechoic chamber in which the test section of the wind tunnel is installed. The chamber is ISO 3745 norm commissioned for a cut-off frequency of 160 Hz. The wind tunnel has a 0.9×0.7 m^2 rectangular test section, with a maximum flow speed of 60 m/s and a turbulence intensity below 0.1 %. Detailed information about the wind tunnel and the facility can be seen in [1].

2.1.2 Far-field acoustic microphone arrays

Two arrays were set up to assess the directivity patterns of the propeller noise: a linear and an arc array. The linear array consists of 10 microphones positioned parallel to the flat surface. The central microphone of the array is located at a 1.5 m (4.9 D) distance from the propeller center. The microphones are separated from each other by 0.15 m. The microphones are positioned, respectively (from upstream to downstream): 63°, 68°,73°,79°,84°,90°,96°,101°,107° and 112°. The second set of microphones is a 1.5 m radius arc array positioned at the top of the propeller, perpendicular to the flat plate. It consists of 17 microphones $(40°, 50°, 55°, 60°, 65°, 70°, 75°, 80°, 90°, 100°, 105°, 110°, 115°, 120°, 125°, 130°, 140°)$. The acoustic measurements were done using G.R.A.S.40 PH free-field microphones.

2.1.3 Hotwire Anemometry

Using hot-wire anemometry (DANTEC's StreamLine Pro CTA) and a single-wire probe (55P15), the boundary layer characteristics at the propeller's plane were evaluated.

2.1.4 Near-field instrumentation

Unsteady pressures are acquired using an instrumented plate beneath the propeller. The plate acquires the pressure by 0.5 mm diameter pinholes attached to a remote microphone probe (RMP) setup through a 1.6 mm channel. Each pinhole leads to a *Knowles FG-23329-P07* microphone. Those microphones are connected to a *PXIe-4499* Sound and Vibration module (NI PXIe-1073 chassis). Steady pressures are measured by connecting the anechoic end of the RMP setup to the pressure scanner *NetScanner 9216*.

2.1.5 Performance and RIG instrumentation

The propulsive system rig consists of an electric brushless DC motor *SCORPION SII-4035-330KV* (2400 W, KV330) connected to the propeller through an 8mm shaft. The back end of the motor shaft is connected to an encoder *HENGSTLER ACURO AD35* (22-bit single-turn, absolute encoder). The motor-encoder set is connected to a *FUTEK MBA500* bi-axial load cell (222 N; 5.65 Nm) through a metal piece which is used for the thrust measurement. The power to run the ESC-Motor is provided by a Delta Eletronika SM3300 (100 V / 75 A). Figure 1 shows the schematics of the rig.

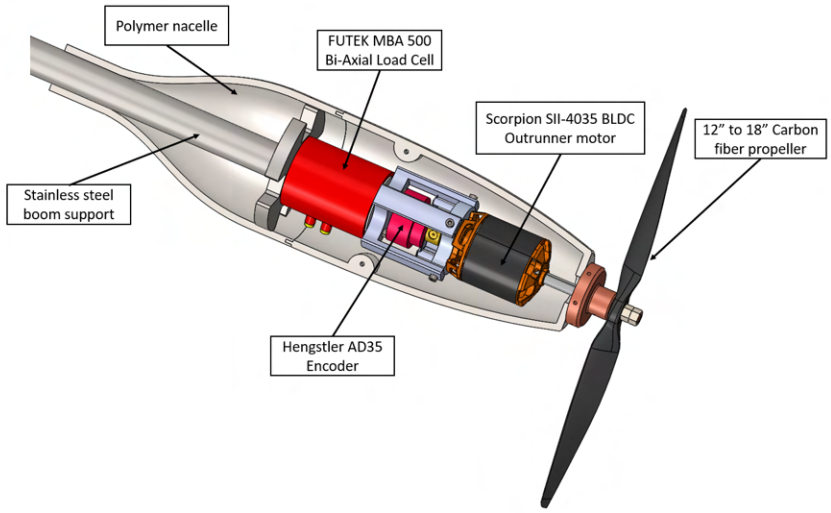


Figure 1: Propulsive system schematics.

2.2 A1 Experimental Campaign UTWE

2.2.1 Overview

The experimental campaign executed in UTWE had the objective of gathering acoustic data of propellers under boundary layer ingestion (Configuration A1). The propeller is positioned close to the bottom wall of the semi-open section of the UTWE wind tunnel (5 mm clearance), to ingest the incoming flat plate boundary layer. Data acquisition is done with microphone arrays - positioned on the far field - and an instrumented flat plate underneath the propeller - near-field. Figures 2 and 3 show the schematics of the configuration.

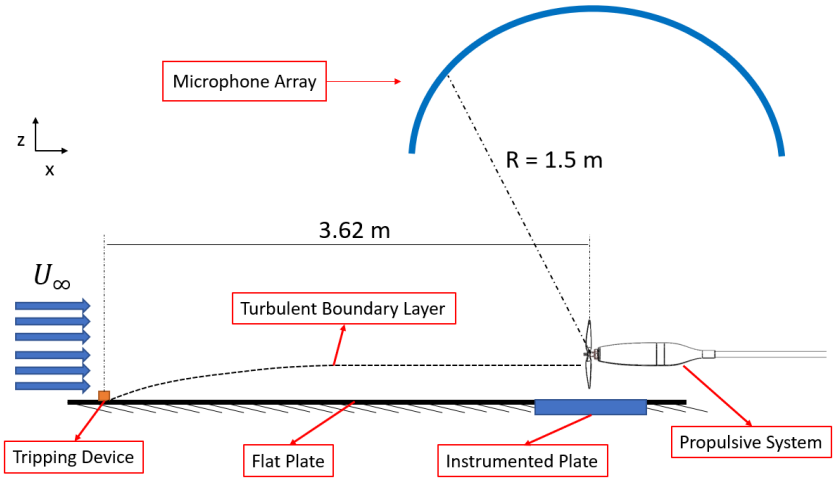


Figure 2: UTWE experimental setup (side-view).

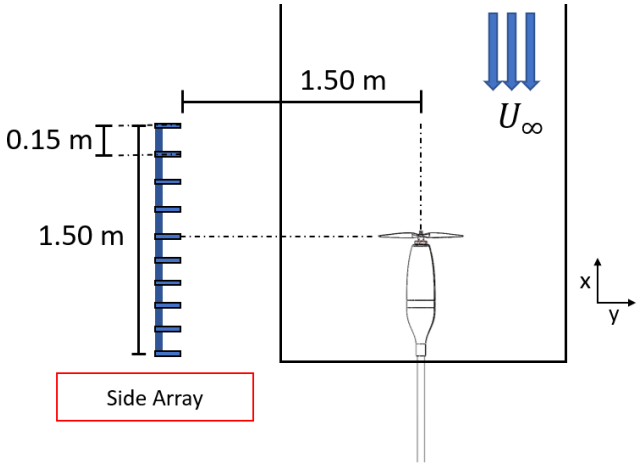


Figure 3: UTWE experimental setup (top-view).

2.2.2 Boundary Layer

The boundary layer impinging on the propeller is controlled by 60° zigzag tripping devices positioned 3620 mm upstream of the propeller plane. The tripping device height controls the boundary layer thickness. Trip 0 is the flat plate only. Trip 1 and Trip 2 have 8 mm and 12 mm trip heights, respectively. The boundary layer thickness in each experiment determines the immersion level of the propeller blades. An immersion ratio ranging from 18% to 45% is possible. Table 1 shows the main characteristics of each boundary layer at the propeller plane.

Table 1: A summary of the boundary layer properties of the three trips as measured at the propeller plane without the propeller (A1, UTWE)

Trip Name	BL Thickness ($\delta_{99\%}$)	Displacement Thickness (δ^*)	Momentum Thickness (θ^*)
Trip 0	56.5 mm	7.0 mm	9.0 mm
Trip 1	102.5 mm	8.7 mm	11.1 mm
Trip 2	139.8 mm	14.5 mm	18.0 mm

2.2.3 Instrumented flat plate

The instrumented flat plate underneath the propeller acquires the steady and unsteady pressure of the surface. The pinholes are distributed exponentially so that the span-wise correlation length can be assessed. The pinholes are connected to the microphones through flexible tubes that are calibrated using a methodology described in [2]. Figure 4 shows the schematic of the plate with the positions of the pinholes.

2.2.4 Test matrix

For the experimental campaigns, the baseline configuration is set at the center of the wind tunnel (no immersion in the boundary layer). Boundary layer ingestion experiments were done with a baseline clearance - the distance between the propeller tip and the flat plate - of 5 mm. The conditions of the propeller are $U_0 = 30$ m/s unless told otherwise. The experiments vary those conditions, to get a detailed understanding of the performance and acoustics of the propeller. Table 2 shows an overview of the parameters tested and the instrumentation used in each experiment.

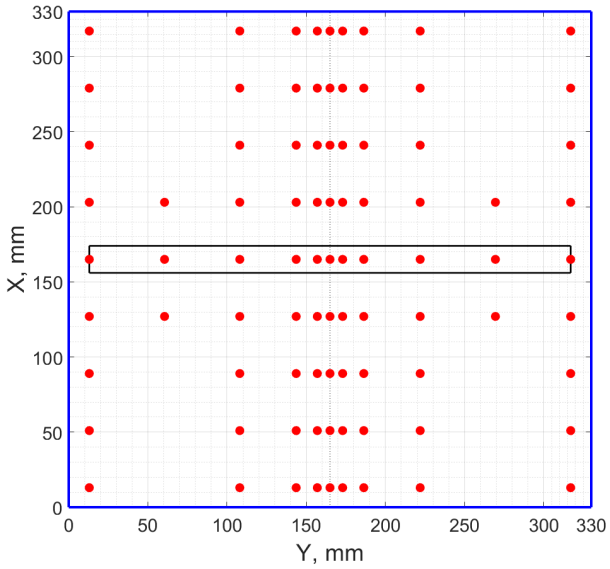


Figure 4: Instrumented plate pinhole positions (top view, x-y plane). X is the stream-wise direction and Y is the span-wise direction. Flow goes from top to bottom. Red circles represents the pinhole positions. Central rectangle shows the propeller wetted area.

Table 2: Summary test matrix of UTWE experiments. J is the advance ratio and U is the wind tunnel speed.

			Instrumentation			
	Conditions		**Onboard**	**Array**		
Session	**Trips**	**Variables**	**Load Cell**	**Instr. Plate**	**Polar Array**	**Linear Array**
Far-field Acoustics	0, 1 and 2	J, U			x	x
Near-field Acoustics	0, 1 and 2	RPM, U, Clearance	x	x		
Load Cell	0, 1 and 2	RPM, U	x			
Static Pressure	0, 1 and 2	RPM, U, Clearance		x		

2.2.5 Database structure

The published database for UTWE Configuration A1 follows the structure shown in Figure 5. The directories are divided into folders for each different dataset. *Time series* data refers to raw data acquired in the time domain. *Processed* data refers to data that were treated (calibrated, corrected, etc.) and processed (Spectral density, time-averaged, etc.). The *Complementary* folder has all schematics and important distances to analyse the data.

All folders contain a README file with a metadata explanation. Additional files with calibration information and also routines to convert and extract the data are also provided. The data can be seen at the DOI `https://doi.org/10.5281/zenodo.7940856`

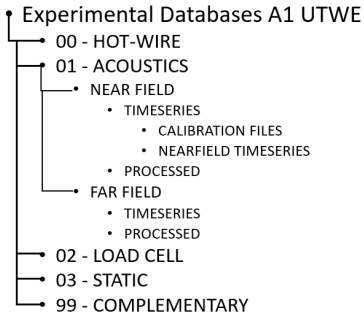


Figure 5: Directory tree of A1 database (UTWE)

2.2.6 A1 CAD Geometry Database

The complete geometry for the UTWE A1 setup is provided and available in the Zenodo database. The full setup is provided, set in the baseline configuration - distance between blade tip and flat plate of 5 mm, and distance between propeller plane and end of contraption of 3200 mm. Also, CAD for the separated components were also supplied. The geometries are in the Zenodo repository file named "A1 CAD UTWE.zip".

3 A - UBRI

This section presents the experiments conducted at the University of Bristol, regarding the A1 and A2 configurations. Firstly, instrumentation specifications common to both A1 and A2 configurations are described. Followed by the plate instrumentation, test matrix, published data, and the database DOI for the respective configurations. Inlcuded in this report are links to the CAD geometry

3.1 Aeroacoustic Facility

3.1.1 Anechoic chamber and wind tunnel

The aeroacoustic facility at the University of Bristol is a temperature-controlled, closed-circuit, open-jet anechoic wind tunnel. The open jet has exit dimensions of 775 mm in height and 500 mm in width, and can achieve free-stream velocities of up to 40 m/s. The free-stream is highly uniform across its exit plane with 0.12% unfiltered turbulence intensity across the jet core. The settling chamber, contraction nozzle, test section, and collector are located inside an anechoic chamber that measures 7.9 m in length, 5.0 m in width, and 4.6 m in height. The chamber is anechoic down to 160 Hz. For further details regarding the design and performance of the aeroacoustic wind tunnel facility, the reader is referred to Mayer et al. [3].

3.1.2 Far-field acoustic microphone arrays

The far-field acoustics were measured using two polar microphone arcs, placed overhead and to the side of the A1 and A2 setups. The overhead arc has 23 microphones with polar angles from $\theta = 40°$ to $\theta = 155°$ in 5° increments (note that only 21 are used during the A1 tests). The orthogonal side array has 25 microphones spanning from $\phi = 25°$ to $\phi = 145°$ in similar increments. The exact positioning of the arcs is detailed in the Supplementary files in the database. The microphones used are GRAS 40PL free-field microphones that are factory calibrated and have a flat response up to 10 kHz.

3.1.3 Hotwire Anemometry

In this test campaign, both 1-D and 2-D hotwire probes were used to quantify the flow field behaviour. The probes used were the Dantec 55P14, 55P15, 55P16, 55P61, and 55P63 probes connected to a Dantec Streamline Pro CTA system. The probes were calibrated before each measurement session using a Dantec Dynamics Hot-Wire Calibrator. The probes were then mounted on arms attached to a 3-axis ThorLabs LTS300M traversing system to allow precise and repeatable probe positioning.

3.1.4 Near-field Instrumentation

Near-field instrumentation comprised of static pressure taps and wall pressure transducers embedded in the A1 and A2 plates. Static pressure taps are 1.6 mm diameter brass tubes that are mounted flush with the plate surface. The tubes are then passed to Chell μDAQ 32-channel pressure scanners which record the static pressure values that are then sent to a PC over TCP/IP. The wall pressure transducers used for measuring the unsteady wall pressure fluctuations were the Knowles FG-23329-P07, which were connected to a signal conditioner. The sensors were calibrated in situ using a reference GRAS 40PL microphone. The transducers were encased in a 3D-printed cap to reduce the sensing port to 0.4 mm in diameter and to ease installation. Figure 6 shows how the instrumentation was embedded in the plates' surfaces.

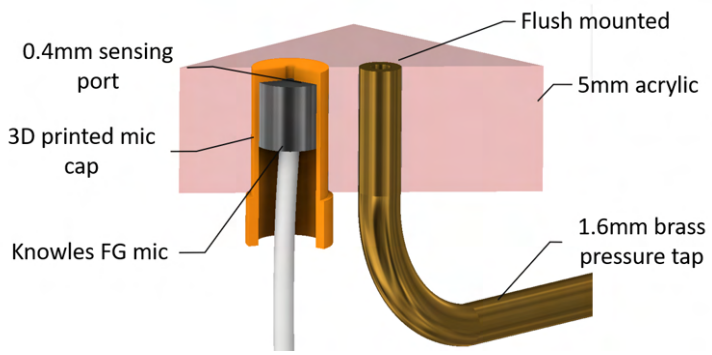


Figure 6: Example of how the near-field static pressure taps and surface pressure transducers are installed, shown here in the A1 plate.

3.1.5 Propeller Rig

The purpose-built propeller rig houses a number of key instruments and technologies to aid the test campaign. To measure the propeller thrust and torque, a 6-axis ATI mini40 load cell is used. The blade position is registered by an RLS RE36 Absolute Rotary Encoder, mounted to the rear of the motor system, and coupled to the motor shaft. Two brushless DC motors were used in this setup, the first is a 2.7kW Scorpion SII-4035-250kV motor used in the A1 tests, and the second is a 3.2kW T-Motor AT4130-300kV motor used in the A2 tests, both driven by a Scorpion Tribunus II 12-80A electronic speed controller. Throughout this data collection campaign, the propeller used was a 12x18" carbon fibre Mejzlik two-bladed propeller. An aerodynamic nacelle structure, manufactured from aluminium, enclosed the motor and the aforementioned instruments, which was then mounted on a solid aluminium and steel support structure. This structure includes a rail-carriage traversing system to allow the propeller position to be varied spanwise (*i.e.*, perpendicular to the plate surface). The traverse motion was controlled by a ThorLabs LTS300M linear stage. The propeller rig also included a cooling system by way of injected compressed air, cooled using a Ranque-Hilsch vortex tube. The internal structure of the propeller rig is seen in Fig. 7. The cooling system exhausts the air from the rear of the rig.

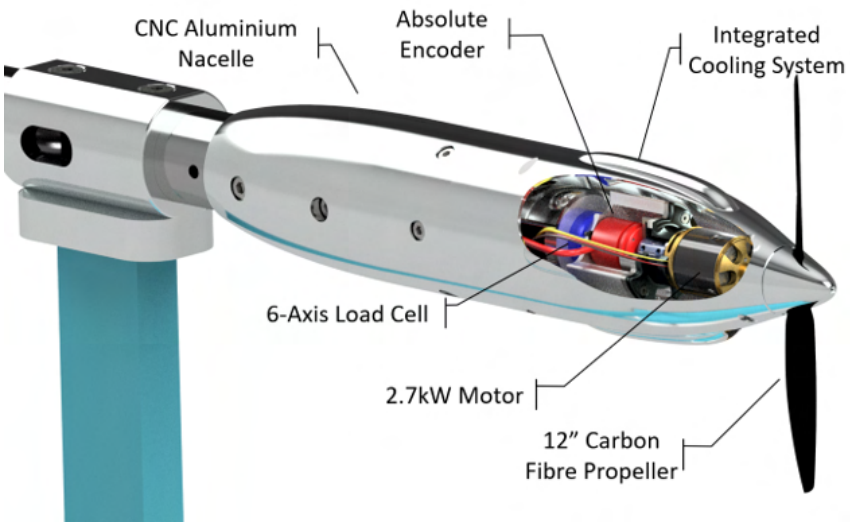


Figure 7: Internal structure of the propeller rig

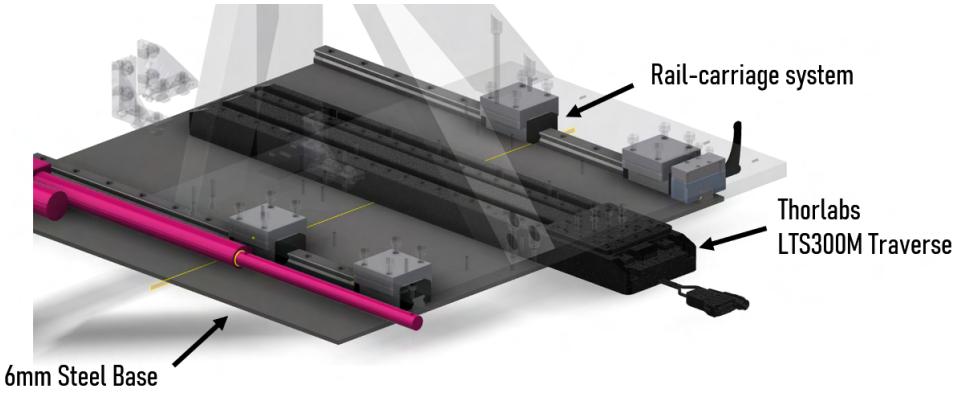


Figure 8: Traversing system used to vary the propeller-plate gap

3.1.6 Control and Data Acquisition System

Closed-loop motor control and synchronised data acquisition were achieved by routing all acquisition devices through PXIe-4499 and PXIe-6341 cards mounted in a single National Instruments PXIe-1082 chassis running from a single sample clock, which is connected to a desktop PC and commanded by LabVIEW control and acquisition software. The only exceptions to this are the Chell pressure scanners which communicated over TCP/IP. In this case, synchronicity was achieved by pulsing the scanners with the same sample clock signal that is set by the NI chassis. Signals from the load cell, near-field pressure transducers, far-field microphones, absolute encoder, hot-wire measurements, RPM tachometer, and motor PWM outputs were all acquired and monitored through this system to ensure the consistency, reliability and repeatability of the results. The data was acquired and simultaneously streamed direct-to-disk in the binary TDMS format. These files were then processed in Matlab to produce the HDF5 datasets.

3.2 A1 - UBRI

3.2.1 Overview

The A1 configuration has been designed to replicate the ingestion of a zero-pressure gradient boundary layer by a propulsion system, in this case, a two-bladed propeller. The setup comprises of a 2x1.69 m acrylic plate mounted adjacent to the wind tunnel nozzle exit. The propeller is then placed 1 m metre downstream of the nozzle exit and the blade tip-to-plate distance is 5 mm. This tip gap distance is the default value during RPM sweeps and hotwire measurements, during tip traversal studies (to see the effect of tip gap), this value is then varied accordingly. Figure 9 shows the layout of the experimental setup for configuration A1. The incoming flow is tripped using three different tripping devices to trigger the development of boundary layers with varying thicknesses and turbulence characteristics upstream of the propeller. The tripping devices are placed at the nozzle exit, the resulting boundary layers are described in Sec. 3.2.3.

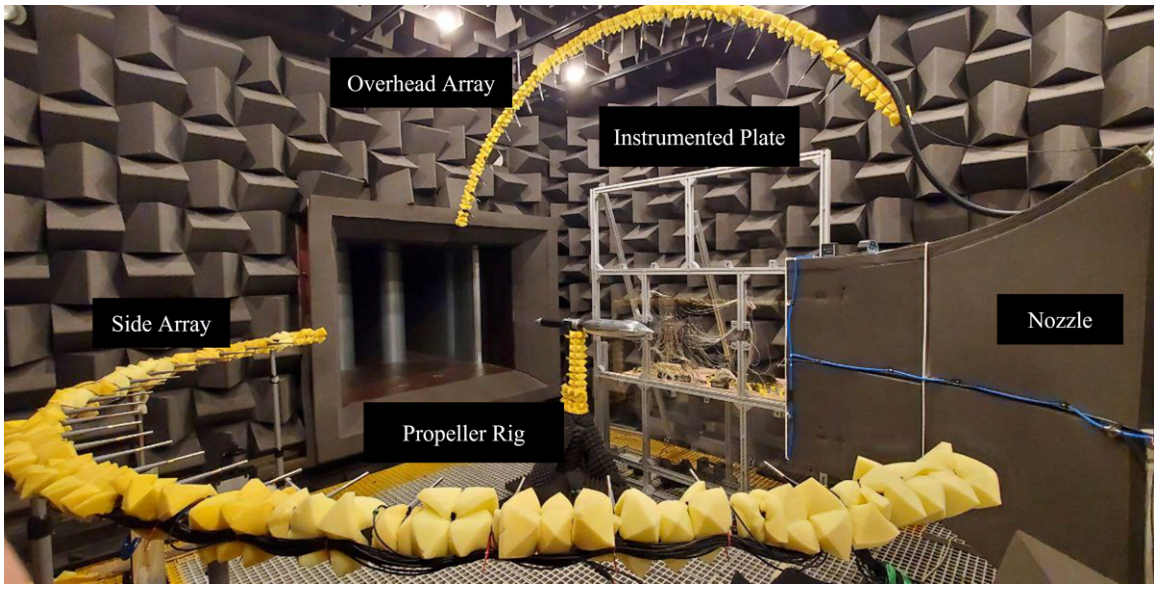


Figure 9: Layout of the experimental setup for the A1 configuration inside the Aeroacoustic Facility

3.2.2 Flat Plate Instrumentation Distribution

As described in Sec. 3.1.4, near-field instrumentation consists of static pressure taps and wall pressure transducers. The A1 plate has 112 pressure taps and 69 wall pressure transducers distributed both in streamwise and spanwise directions. A diagram of the instrumentation layout is seen in Fig. 10. The full coordinates of each sensor are contained within the dataset. It should be noted that while 112 pressure taps were installed in the plate, only 96 were used due to channel limitations.

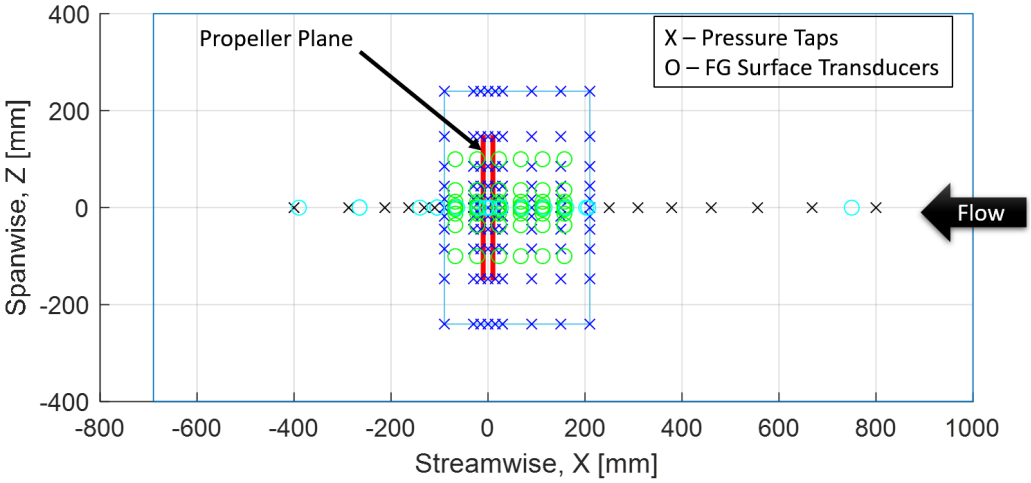


Figure 10: Distribution of surface instrumentation for configuration A1

3.2.3 Test Matrix

The variables investigated for the far-field noise (non-hotwire) measurements include the propeller RPM, tip gap, and boundary layer thickness. Boundary layer characteristics were determined via hotwire anemometry measured at the propeller location without the propeller and the resulting boundary layer characteristics can be seen in Table 3. The three boundary layers tested were produced using three trips, A,B and C. Trip A consisted of a strip of 80-grit sandpaper 25 mm in width, Trip B consisted of a strip of porous iron foam measuring 5 mm in height and 50 mm in width, the foam has a porosity of $\varphi = 85.37\%$, corresponding to 45 pores per inch (PPI). The third trip was a coarse uncompressed porous metal foam (Trip C), which is 25 mm wide and 10 mm thick with a porosity $\varphi = 90.92\%$, equivalent to 25 pores per inch (PPI) [4, 5]. Due to the large number of sensors, the acoustic tests for each operating condition were performed twice, with the first obtaining data from both far-field arrays, and the second focusing on collecting the near-field data. Several far-field microphone results were collected simultaneously for the latter to help correlate the near-field hydrodynamic field to the far-field acoustics. The free-stream velocity is fixed at $U = 30$ m/s. The acoustic test matrix is seen in Tables 4 and 5. The load cell is highly sensitive to small changes in temperature and so dedicated runs to quantify the aerodynamic performance for each condition of interest were performed separately to improve load measurement accuracy.

Table 3: A summary of the boundary layer properties of the three trips as measured at the propeller plane without the propeller, A1, $x = 0m$

Trip Name	99% Thickness ($\delta_{99\%}$)	Displacement Thickness (δ^*)	Momentum Thickness (θ^*)
A - Sandpaper	20.5 mm	2.7 mm	2.1 mm
B - Thin	42.5 mm	4.5 mm	3.6 mm
C - Thick	101 mm	12.2 mm	9.8 mm

Table 4: Table showing test matrix of acoustic BLI experiments for A1 UBRI (*x,3 mics* means only 3 microphones were connected)

	Conditions		Instrumentation			
			Onboard		Farfield	
Session	**Trips**	**RPMs**	**Encoder**	**Load Cell**	**Overhead Arc**	**Side Arc**
Far-field Acoustics	ABC	Full Sweep			x	x
Near-field Acoustics	ABC	Full Sweep	x		x	x, 3 mics
Load Cell Runs	ABC	Detailed Sweep		x		
Far-field Acoustic Traversed tip gap	ABC	Selection 1	x		x	x
Near-field Acoustic Traversed tip gap	AC	Selection 1	x		x	x, 3 mics
Load Cell Traverse Runs	ABC	6500, 8100		x		

Table 5: Table showing acoustic test matrix of BLI experiments for A1 UBRI (continued)

	Conditions		Instrumentation	
			Nearfield	
Session	**Trips**	**RPMs**	**Surface microphones**	**Static pressure**
Far-field Acoustics	ABC	Full Sweep		
Near-field Acoustics	ABC	Full Sweep	x	x
Load Cell Runs	ABC	Detailed Sweep		
Far-field Acoustic Traversed tip gap	ABC	Selection 1		
Near-field Acoustic Traversed tip gap	AC	Selection 1	x	x
Load Cell Traverse Runs	ABC	6500, 8100		

Table 6: Definition of RPM Selections used in Table 4

RPM sets definition	
Full Sweep	4100:200:8300, 8700, 9000, 9500, 10000
Detailed Sweep	3500:100:4300, 4500:200:8300, 8700, 9000, 9500, 10000
Selection 1	5100, 6500, 8100

In addition to the acoustic test matrix, hotwire anemometry was performed at key locations for one condition (J=0.91, 6500 RPM) to allow WP4 partners to initialise and validate their numerical simulations. The hotwire data was gathered as described in Sec. 3.1.3. In addition to the assessment of the boundary layer velocity profiles using single-wire probe (note that single-wire probe measures the total velocity of the incoming flow), two-component cross-wire probes were used to provide knowledge of x- and y-velocities and their fluctuations at three different streamwise locations along the flat plate when the propeller is running. At each location, the measurement begins from the closest distance (permissible by the hot-wire set-up) from the wall and vertically extends beyond the full remit of the propeller (*i.e.*, a line measurement). Full details on the location and sign conventions can be seen in the Supplementary files in the database. Line 1 is measured 10cm from the nozzle exit, Line 2 is measured 1 propeller diameter (D) upstream of the propeller and Line 5 is measured 1D downstream of the propeller. Lines 3 and 4, are placeholder names that were not performed.

3.2.4 Database structure

The configuration A1 dataset is structured as shown in Fig. 11. There are three top-level directories, 'Processed' contains the acoustic, pressure, and hotwire measurements in statistical quantities i.e., mean, Power Spectral Density, rms etc. README files are present inside each directory describing the data structure and variables of the files within. 'Supplementary' contains information on the experimental layout of the setup, including arc positioning, 'Timeseries' only contains the timeseries for the hotwire measurements and not other measurements due to upload restrictions. All data is in engineering units, and all sensitivities and calibrations are applied. A thorough reading of the README files is recommended. The DOI for both the UBRI A1 and A2 database is `https://doi.org/10.5281/zenodo.7924655`.

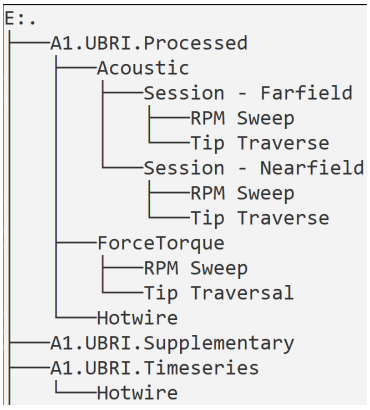


Figure 11: Directory tree of the A1 database (UBRI)

3.2.5 A1 CAD Geometry Database

The geometry of the A1 setup is provided as part of this deliverable. The design CAD files were cleaned and made watertight to allow a simpler meshing process for CFD usage. Features such as sensor holes, bolt holes and material seams were removed. All internal voids are also filled. The main components of the setup are supplied as separate STEP files as well as a single STEP file that represents the default arrangement i.e., $x = 1$ m with a tip gap of 5 mm. The components supplied as separate files are the propeller rig, the propeller, the wind tunnel nozzle, and the flat plate. They are contained in the file named *"A1.CAD Geometry.zip"* in the Zenodo database.

3.3 A2 - UBRI

3.3.1 Overview and Schematic

The A2 experimental setup has been designed to create an adverse pressure gradient boundary layer which is then ingested by a propeller. This is similar to installation configurations where the propulsion system is partially buried in the fuselage of an aircraft. The setup consists of an S-shaped plate mounted adjacent to the wind tunnel nozzle exit, similar to the A1 configuration. The curved section of the plate is defined by a cubic Bezier function with control points: Points $=[0, 0.2; 0.75, 0.2; 0.25, 0; 1, 0]$. The propeller rig is positioned at a streamwise location downstream of the nozzle exit. This streamwise location is varied during the tests. The flow is tripped with 80-grit sandpaper to initiate the development of a boundary layer which flows over the curved section of the plate, generating an adverse pressure gradient. The plate measures 1.69 m x 2 m and was made up of a thin plywood sheet formed over a CNC-cut plywood skeleton support structure which was in turn mounted on aluminium profiles. The trailing edge of the plate was lined with porous material to reduce trailing edge effects.

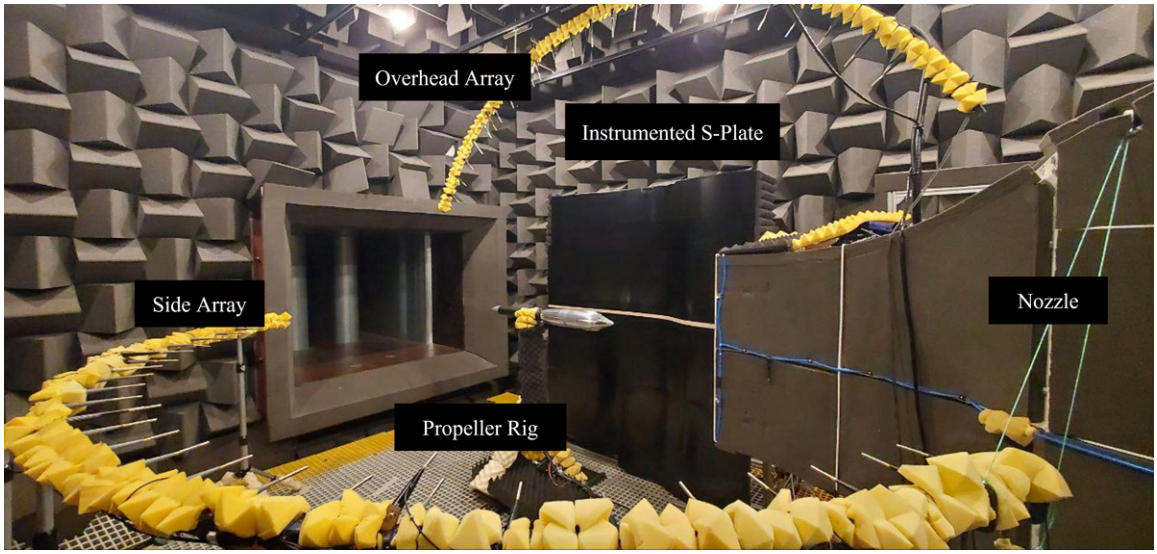


Figure 12: Layout of the experimental setup for the A2 configuration inside the Aeroacoustic Facility

3.3.2 S-Plate Instrumentation Distribution

As described in Sec. 3.1.4, near-field instrumentation consisted of static pressure taps and surface pressure transducers. The A2 S-plate has 32 pressure taps and 24 surface pressure transducers distributed along the streamwise centreline. The instrumentation layout is seen in Figs. 13 and 14.The wall pressure transducers are placed in streamwise pairs – full coordinates of each sensor are contained within the dataset. The coordinate system used in this dataset is defined such that X is in the streamwise direction, origin at the nozzle edge +downstream, and Y is positive normal to the plate with the same origin location. The Z direction is defined as spanwise along the plate. Further details on sign conventions and coordinate systems are found in the supplementary files in the database.

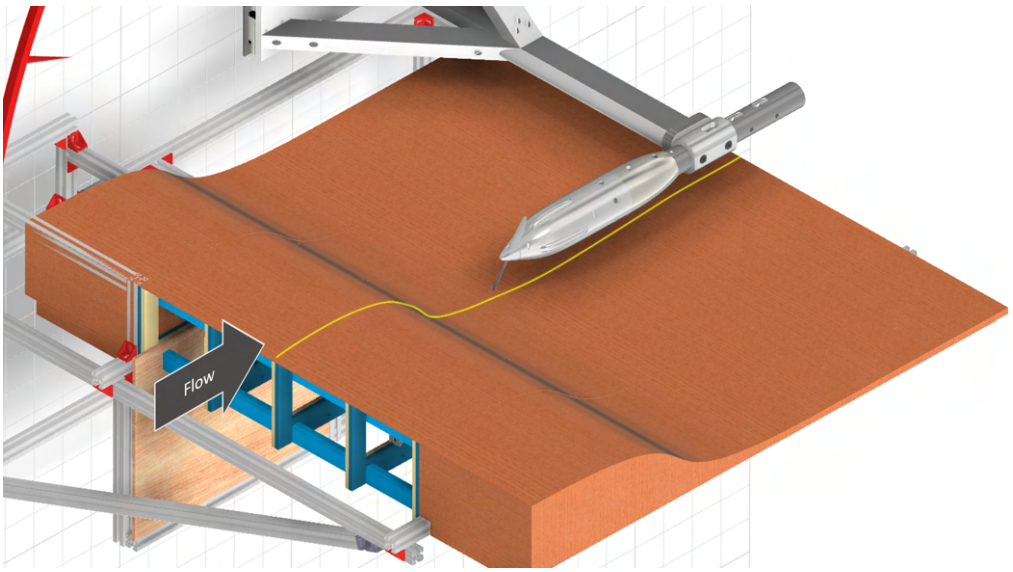


Figure 13: Location of the instrumented streamwise centreline on the A2 plate

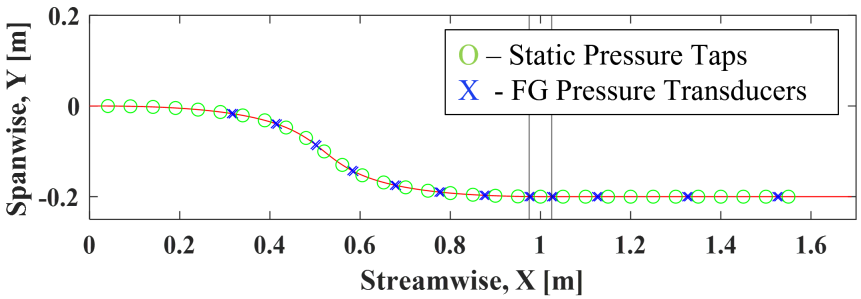


Figure 14: Distribution of surface instrumentation for configuration A2 along the centreline

3.3.3 Test Matrix

The test matrix for configuration A2 consisted of RPM sweeps and tip-gap sweeps for varying propeller streamwise positions and freestream velocities. During an RPM sweep, the propeller progressed through the specified number of RPMs and initiated data acquisition for each speed. During the tip-gap sweeps, the RPM was kept constant and the linear stage controlling the propeller spanwise position was iterated through a number of tip-gap positions with data acquisition being triggered at each step. The full list of tip-gap distances tested can be found in the dataset. These parameter sweeps were performed for different streamwise positions of the propeller, with the default tip-gap distance maintained at 5 mm at each of these positions. The far-field microphones, near-field microphones and pressure taps were all acquired simultaneously, force measurements, similar to A1, were acquired in dedicated 'Performance' runs. The test matrix can be seen in Table 7.

The flow field measurement test matrix consisted of several line measurements, similar to A1, distributed streamwise at one operating condition ($U = 27$ m/s, 6500 RPM). The two-component cross-wire hotwire data was obtained with the propeller operating at 6500 RPM and $U_{inf} = 27$ m/s, the propeller position is 80 cm downstream of the nozzle exit and the tip-gap is 5 mm. Upstream of the propeller, lines were taken at $X = 10, 48, 72$ cm positions, downstream of the propeller a grid of points was taken in the space between the nacelle and plate. Both statistical data and timeseries data are available in the database. Two-component boundary layer assessment lines were measured at the propeller location $X = 80$ cm for the two freestream velocities, $U_{inf} = 25, 27$ m/s with the propeller absent.

Table 7: Table showing the acoustic test matrix for configuration A2

Type	RPM Sweep		Tip Traverse	
Session	Acoustic	Performance	Acoustic	Performance
Propeller Position, X [cm]	48, 80, 100	48, 80, 100	48, 80	48, 80
U_{inf} [m/s]	27, 25	27, 25	27	27
RPM	Full Sweep	Detailed Sweep	Selection 2	Selection 2
Instrumentation				
Encoder	x	x	x	x
Load Cell		x		x
Overhead Arc	x		x	
Side Arc	x		x	
Surface microphones	x		x	
Static pressure	x		x	

Table 8: Table showing the definitions of the RPM sets seen in Table 7 for the A2 configuration

RPM sets definition	
Full Sweep	5100:200:8300, 8700, 9000, 9500, 10000
Detailed Sweep	3500:100:4300, 4500:200:8300, 8700, 9000, 9500, 10000
Selection 2	6500, 8100

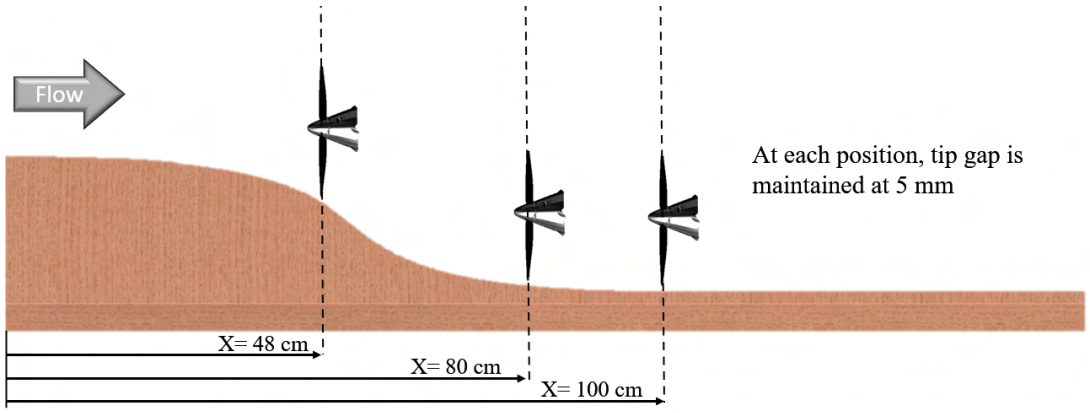


Figure 15: Locations of the three tested streamwise positions

3.3.4 Database structure

The dataset on the A2 configuration is structured as shown in Fig. 16. There are three top-level directories, 'Processed' contains the acoustic, pressure, and hotwire measurements in statistical quantities i.e., mean, Power Spectral Density, rms etc. README files are present inside each directory describing the data structure and variables of the files within. 'Supplementary' contains information on the experimental layout of the setup, including arc positioning, 'Timeseries' only contains the timeseries for the hotwire measurements and not other measurements due to upload restrictions. All data is in engineering units, and all sensitivities and calibrations are applied. A thorough reading of the README files is recommended. The UBRI datasets for both A1 and A2 configurations can be found at `https://doi.org/10.5281/zenodo.7924655`.

```
E:.
├──A2.UBRI.Processed
│   ├──Acoustic
│   │   ├──Background
│   │   ├──RPM Sweep
│   │   └──Tip Traverse
│   ├──ForceTorque
│   │   ├──RPM Sweep
│   │   └──Trip Traverse
│   └──Hotwire
├──A2.UBRI.Supplementary
└──A2.UBRI.Timeseries
    └──Hotwire
        └──DS
```

Figure 16: Directory tree of the A2 database (UBRI)

3.3.5 A2 CAD Geometry Database

The geometry of the A2 setup is provided as part of this deliverable. The design CAD files were cleaned and made watertight to allow a simpler meshing process for CFD usage. Features such as sensor holes, bolt holes and material seams were removed. All internal voids are also filled. The main components of the setup are supplied as separate STEP files as well as a single STEP file that represents the default arrangement i.e., $x = 80$ cm with a tip gap of 5 mm. The components supplied as separate files are the propeller rig, the propeller, the wind tunnel nozzle, and the S-plate. A CSV file containing XY coordinates that describe the curve of the plate is also supplied. They are contained in the file named *"A2.CAD Geometry.zip"* in the Zenodo database.

4 B1 - TUD

This section outlines the results of experiments conducted at Delft University of Technology on configuration B1. It provides a comprehensive overview of the experiments, including information on the wind tunnel, setup characteristics, test conditions, and configurations investigated. Additionally, the section outlines the measurement techniques applied and specifies where the data is available for public use.

4.1 Wind Tunnel Facility

The experiments were carried out at the Low-Speed, Low-Turbulence Tunnel (LTT) located at Delft University of Technology. This wind tunnel is a closed-circuit type with a maximum freestream velocity of $120\,\mathrm{m\,s^{-1}}$ and turbulence levels below 0.04% for the freestream velocity used in these experiments. The LTT aeroacoustic test section (Fig. 17) was used for the experiments described in this section. It is a specially designed section with lined side panels and a microphone array recessed from a Kevlar panel. The test section has an octagonal cross-section with dimensions of 1.25m in height, 1.8m in width, and 2.6m in length. Its floor and ceiling were covered with 3cm Basotect melamine foam during acoustic measurements.

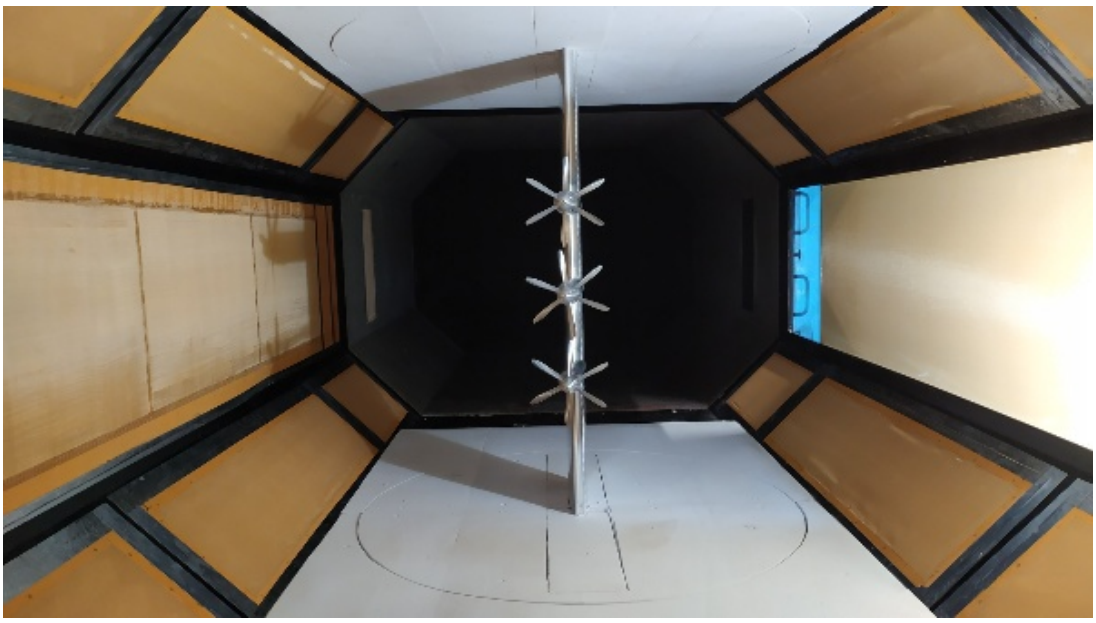


Figure 17: LTT aeroacoustic test section.

Fig. 17 displays a Kevlar window on the right-side panel of the aeroacoustic test section, behind which the microphone array shown in Fig. 18 is placed. The right and left side panels can be switched, allowing acoustic measurements to be taken on both sides.

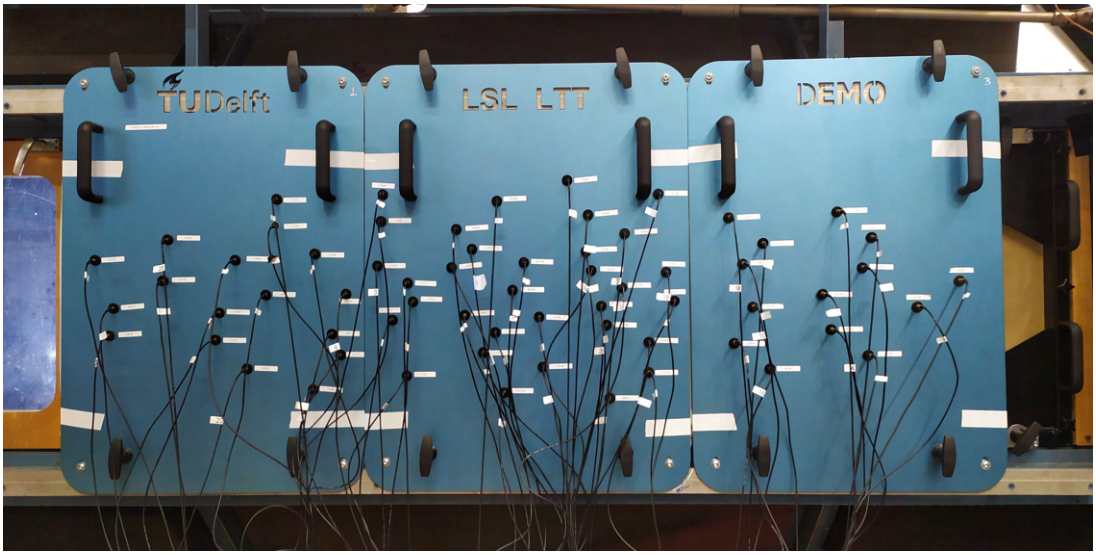


Figure 18: Array of microphones.

4.2 Experimental Setup

The setup consisted of an array of three six-bladed steel propellers, named XPROP-S, with a radius of $R = 101.6$mm. In addition, a fourth propeller, with a mirrored version of the original propeller, was used to invert the rotation direction of the middle propeller and mimic a counter-rotating configuration. These propellers were installed on the leading edge of an unswept, untapered wing model featuring an NLF-Mod22(B) airfoil. The wing has a chord of 0.3m and a span of 1.248m. The propellers were powered by brushless DC electric motors (Lehner LMT 2260/40). Each motor was controlled by a dedicated PWM-controlled trapezoidal electronic speed controller (ESC) and an externally programmable 5 kW DC power supply. The motors were enclosed in an aluminium nacelle, angled downwards at a 5° angle relative to the wing's chord.

4.3 Test Conditions and Configurations

The measurements were conducted at a nominal freestream velocity of 30 m/s. The blade pitch at 70% of its radius was kept at 30°. This pitch angle was preferred over larger angles as it allowed for higher thrust coefficients and blade tip Mach numbers, making it easier to identify both aerodynamic and acoustic interaction effects in the experiment.

Due to the limitations of the electric motor, the propellers were limited at an advance ratio of $J = 0.8$ (184.5Hz), but measurements were also performed at $J = 1.0$ (147.6Hz). The rotational speed and the relative blade phase angle between propellers were controlled with in-house custom-made software. The relative blade angles ranged from 0° to 50° in 10-degree intervals. Random-phase measurements were also performed by increasing the rotational speed of the side propellers by 0.03Hz relative to the middle propeller. This offset corresponds to a change of less than 0.03% in the advance ratio, which has a negligible effect on the propeller's performance. The tip clearance between propellers was 5mm, approximately 5% of the propeller radius. In order to simulate a counter-rotating configuration, the middle propeller was substituted with a mirrored version of the original propeller, as previously mentioned.

The wing's angle of attack ranged from 0° to 10°. Lastly, measurements were obtained using a single propeller mounted on one of the three nacelles to distinguish between interactions with adjacent propellers and interactions with adjacent nacelles. However, due to time constraints, isolated configurations (which involved only one propeller and no adjacent nacelles) were not tested. An overview of test conditions is presented in Table 9.

Table 9: Test conditions and configurations.

Parameter	Evaluated values
Freestream velocity [m/s]	30
Blade pitch at 70% of the blade radius [deg]	30
Advance ratio [-]	0.80, 1.0
Relative blade-phase angle [deg]	random, 0, 10, 20, 30, 40, 50
Rotation direction	co-rotating
Tip clearance [mm]	5
Angle of attack [deg]	0, 2, 5, 8, 10
(P)propeller/(N)acelle configuration	3P + 3N, 1P + 3N

4.4 Measurement Techniques

Three types of measurement techniques were conducted to obtain data on the noise generated by the system, the wing surface pressure, and the slipstream deformation.

A phased microphone array consisting of 64 GRAS 46BE microphones was used to conduct acoustic measurements. The array is elliptical and extends 1.6m in the streamwise direction and 0.4m in the vertical direction. The microphones are recessed 15cm from the Kevlar side wall and are held by a solid plate lined with 5cm plane melamine foam, as shown in Fig. 19. Each measurement lasted 30s and had a sampling frequency of 51.2kHz.



Figure 19: Microphones recessed from the Kevlar wall and held flush with the melamine foam surface.

Pressure taps were utilized to record the wing surface pressure. Two rows of pressure taps were placed in the chordwise direction at 0.7R from the centerline of the middle propeller, as shown in Fig. 20. One row was placed on each side of the wing centerline and had pressure taps in both the upper and lower surfaces of the wing. An electronic pressure scanner with a sampling frequency of 10Hz was used to simultaneously measure all taps, with a measurement time of 5 seconds. The exact location of the pressure taps can be found in the link provided in Section 4.5.

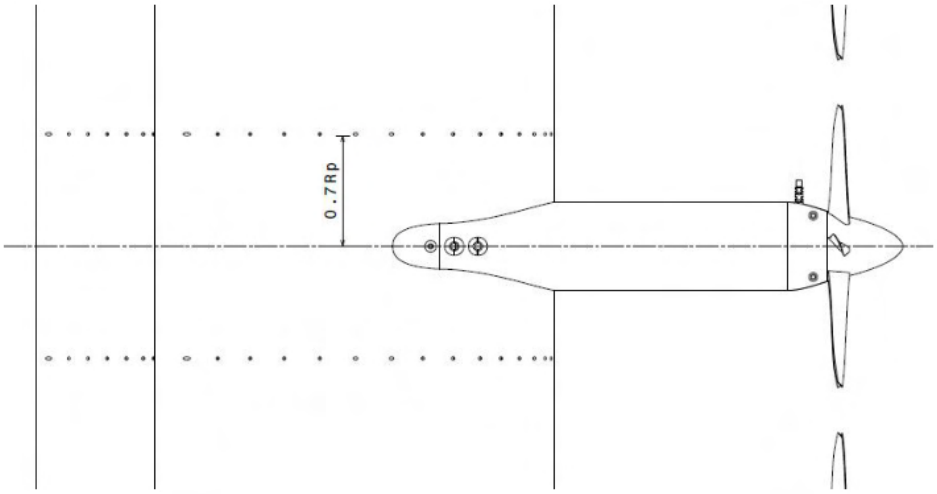


Figure 20: Pressure taps position (top view).

A wake rake equipped with total and static pressure probes (Fig. 21) was used to obtain data on the slipstream deformation downstream of the setup. The wake rake was positioned one chord-length from the wing trailing edge (aligned with the middle propeller) and traversed vertically (in the spanwise direction) at 10mm increments. For the normal direction, the rake was aligned with the centre of the wing wake, and measurements were taken at three positions: −99mm, 0mm, and 99mm from the wake centre. This process provided a resolution of 3mm within 40mm from the test section centerline. The pressure ports were connected to the same electronic pressure scanner used for pressure taps, with the same measurement time. The wake rake and its support rig were used exclusively during the slipstream measurements and were not present in the tunnel at any other time.

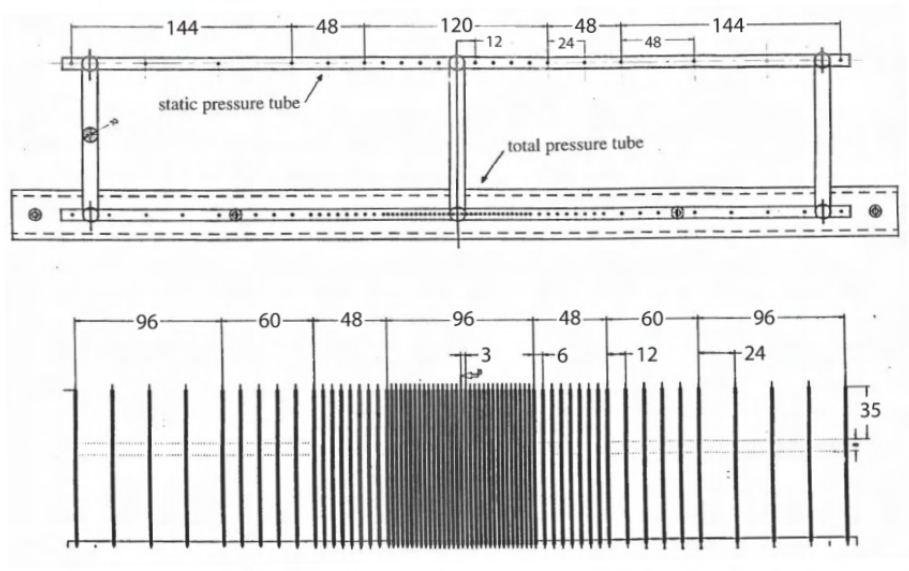


Figure 21: Wake rake with spacing dimensions indicated in mm (front view and top view).

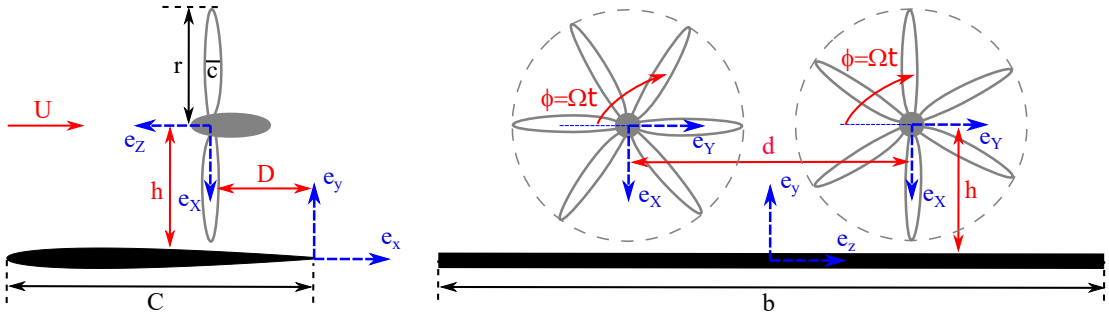
4.5 Data Availability

The configuration B1 dataset is publicly available on the Zenodo repository through the following link: `https://doi.org/10.5281/zenodo.8307371`. It consists of three folders: Acoustics, Aerodynamics, and Geometry, each containing relevant data in acoustic, aerodynamic, and CAD file formats, respectively. The corresponding README and .txt files are also included within each folder.

5 B2-ECL

5.1 Setup Description

The ECL experiment is primarily dealing with the scattering of propeller noise by a wing, for an over-the-wing installation and a pair of side-by-side propellers as shown in Figs. 22 and 23. The configuration, labeled B2 in the project, is a reduced arrangement mimicking DEP systems possibly used in future flying architectures. The experiment is aimed at demonstrating the feasibility of determining an optimum configuration in terms of sound masking by the wing, with regards to observers located below the wing, preserving acceptable aerodynamic performances. Therefore, both the aerodynamic noise and the performances in terms of combined wing lift and propeller thrust must be considered as parameters for the optimization. The space of parameters will be inspected empirically in the study, except for relying on accompanying analytical modeling to identify either promising or detrimental configurations. Several configurations were experimentally assessed, regarding the 5 parameters shown in Fig. 22 and listed in Table 10,



(a) Side view (b) Front view

Figure 22: Schematics of the propellers-wing arrangement, reference frames, and main notations.

Table 10: Setup parametric variations.

	1	2	3
D	0.1r (0.01m)	0.5r (0.05m)	r (0.1m)
h	r+0.1r (0.11m)	r+0.5r (0.15m)	-
d	2r+0.1r (0.21m)	2r+0.5r (0.25m)	-
ϕ	0°	30°	-
U	0 m/s	22 m/s	-

Realistic enough features must be included in the experiment, in order that the search for an optimum makes sense. For this, the two propellers are synchronized, with adjustable phasing in terms of the relative angular positions of the blades. They can be either corotating or contrarotating. Furthermore, the wing-body is a rectangular airfoil, extruded from the cross-section of a true lifting wing of aircraft, namely the F15 shape, with courtesy of DLR. The vertically mounted scattering unswept wing [6] has 0.3 m chord, and 1.4 m total span, for a wetted span of 0.9 m. Additionally, it is set to a non-zero lift angle of attack, kept unchanged in the experiment. The 6-bladed "XPROP-S" propellers from TUD [7, 8], with about

0.2 m diameter and $\gamma = 30°$ blade pitch angle are installed at different positions near the trailing edge, with adjustable separation.

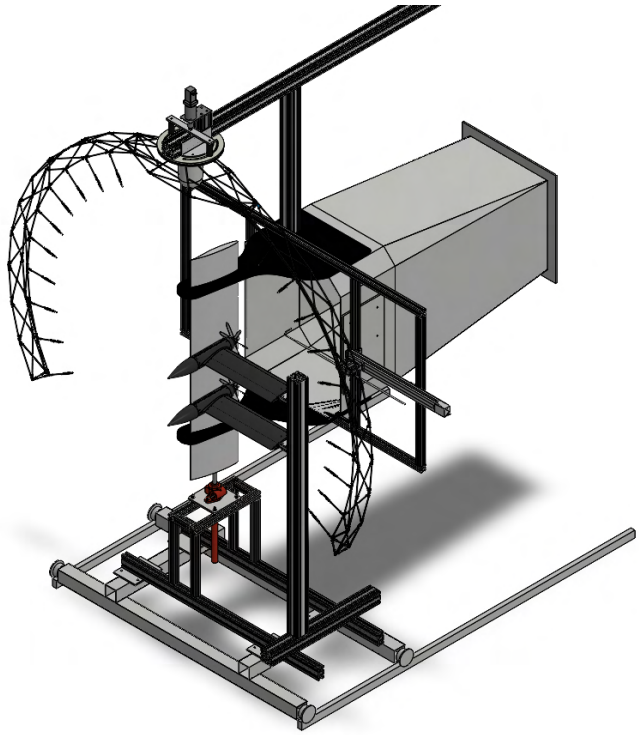


Figure 23: CAD view of the full setup.

Each propulsion unit is made of aligned electric motor, encoder and load cell. The elements are held by mechanical parts fixed to a double hollow beam, in which all cables are gathered. The propellers are powered by two Scorpion SII 4035 250KV motors up to a speed regime of 7000 RPM, corresponding to a blade-tip Mach number of about 0.22. The rotating part of the motor is the external black part in Fig. 24-left, on which an extension is fixed to receive the propeller. A copper coil inserted in an aluminum part is embedding the ODrive encoder with 0.2° accuracy which is used for the propeller synchronization. The ends of the coil, seen in the figure, can be connected to long plastic tubes connected to a pump. Continuous circulation of water ensures the cooling of the assembly. The shroud embedding the complete core assembly is 3D-printed. It includes a beam shroud based on a NACA-type design, as well as an axisymmetric center body ending with a profiled back-end (Fig. 24-right). The hollow shroud also allows to include an accelerometer and a thermocouple, for vibration and temperature control.

A close-up of the pair of propellers installed close to the wing, with the shroud removed, is shown in Fig. 25. The figure also shows the instrumented part of the wing, with two lines of pressure taps, made of pinholes at the end of tubes that are spanwise-inserted in the body of the wing, and connected to an external multi-channel manometric system. The two lines are slightly oblique with respect to the chord direction to avoid wake effects between adjacent pinholes. Making the wing slide through its supports allows to scan the wall pressure and reconstruct a complete pressure-coefficient map.

The main relevant geometrical and operational parameters of the setup are summarized in Table 11.

5.2 Dimensional Considerations

A basic dimensional analysis allows to identify the most determinant parameters of aerodynamic and geometrical natures, to be investigated. The main flow parameters are the mean velocity of the flow delivered by the nozzle, U_0, characterizing the equivalent flight speed of the wing-propeller system, and



Figure 24: Core assembly of a propulsive unit (left) and installed-on-shroud propeller (right). The encoder is hidden by the coil of the water-cooling system.

Table 11: Geometrical and operational parameters.

Parameter	Value
Maximum flow velocity	22 m/s
Wing chord	0.3 m
Propellers diameter	0.205 m
Propellers sweep angle	30°
Number of blades	6
Propellers tip Mach number	0.22
Propellers RPM	7000 rev/min
BPF	700 Hz

the rotational speed Ω of the propellers, assumed the same for both. U_0 and Ω define the advance ratio $J = \pi U_0/(\Omega R_t)$, if R_t is the blade tip radius. Once the geometrical description of the propellers is specified, the application of standard BEMT (Blade-Element Momentum Theory) provides values of the induced speed v_i and other details, such as the angle of attack on the blades, for any selected annulus of the propeller disc. The theoretical thrust and torque can also be obtained. Because the tonal noise, considered as of major interest, is interferential in essence, the sound field must be explored in a three-dimensional way, making two observation angles θ and ϕ, for instance spherical-coordinate angles with respect to an origin taken close to the sources, parameters of interest. The dual propeller system is defined by the axis-to-axis distance D. Its positioning with respect to the wing is defined from the wing trailing edge point at mid-wetted span, by the streamwise distance to the edge d and the normal-to-wing distance h. Because the blades are unswept and radially aligned, the mid-chord plane of the propellers and the plane containing the propeller axes are taken as references for the definition of these distances. For physical consistency, h is measured from the local wing surface point normal to the considered streamwise position. A typical chord length c of the blades is another involved parameter, whereas the full span L can be assimilated to the tip radius for dimensional considerations, in view of the large aspect ratio.

At any observation point, the rms sound pressure can be *a priori* expressed in a dimensionless form as a function of a series of parameters, say

$$\frac{p_{rms}}{\rho_0 c_0^2/2} = \mathcal{F}\left(\mathcal{R}e, M_t, J, k_B, \theta, \phi, k_B R, k_B h, k_B d, \frac{D}{R_t}, m, \frac{\Delta}{R_t}\right) ,$$

where θ and ϕ are the observation angles, R is the observation distance, ρ_0 is the mean fluid density, c_0 the sound speed and $M_t = \Omega R_t/c_0$ the blade-tip Mach number. $\mathcal{R}e = Uc/\nu$ is the Reynolds number

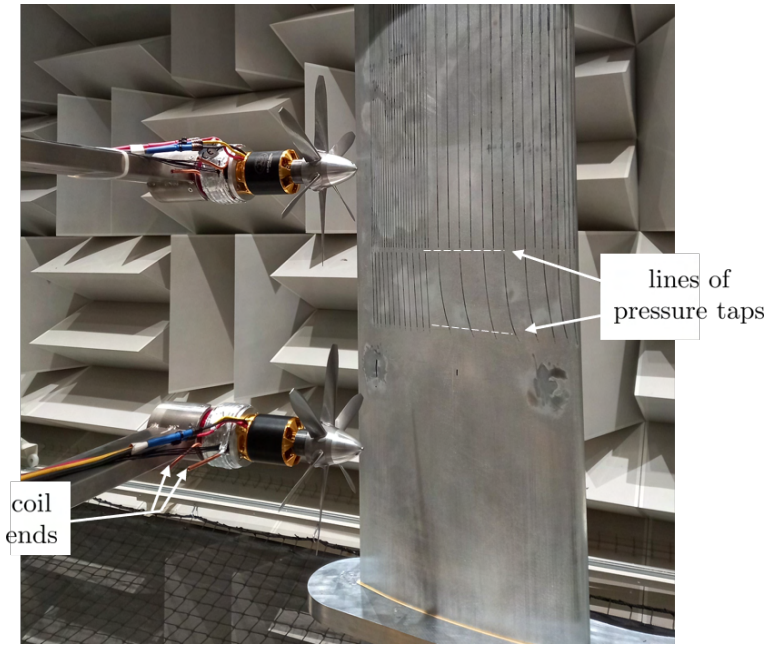


Figure 25: Wing and installed propellers, shroud removed.

built on the blade chord c and the relative speed U (a function of Ω and U_0), at some reference radial position, usually chosen as a percentage of R_t. It is representative of the flow regime around the blades, and is usually low for the present application, entering the transitional range. M_t and J determine the axial-flow Mach number $M_0 = U_0/c_0$. $k_B = B\Omega/c_0$ is the acoustic wavenumber at the Blade-Passing Frequency (BPF), and m the BPF harmonic order.

The functional form $\mathcal{F}$ is *a priori* unknown, the experiment is a way to partially determine it. The number of its dimensionless arguments can be defined rigorously by the Vaschy-Buckingham theorem, provided that a reasonably reduced exploration space of variables is previously identified. But the definition of the parameters is arbitrary; they could be replaced by some combinations of them, at a constant total number of parameters (for instance, M_0 could be selected in place of M_t). The dependency on $k_B R$ can be suppressed for an observer in the acoustic far-field, by virtue of the decrease with inverse distance $1/R$ ensuring similarity. Furthermore, the Reynolds and Mach numbers, as well as the advance ratio, are varied in a limited range. The maximum tangential Mach number is about 0.2 at 7,000 rpm. The instrumentation is designed in such a way that acoustic measurements are performed globally on a portion of sphere, for fixed values of the flow and propeller positioning parameters. All values of m are accessed, as well as, implicitly, the broadband noise.

The present experimental setup allows to explore effects of Ω, J, Δ, h, D and d, for the 6-bladed propellers, on the acoustic signature. A similar analysis can be roughly outlined for the aerodynamic performances. This means that the combined lift of the wing and thrust of the propellers, on the one side, and wing drag and propeller torque, on the other side, must be considered together. They are functions of the same set of parameters. In view of its size, the addressed 6-dimensional space must be bound. Limits are imposed by the installation itself, and by an *a priori* estimation of what is acceptable in terms of aircraft design.

One of the key points to be addressed about sound scattering by the trailing edge is the possible amplification of dipole radiation for compact distances of the sources to the edge. According to Roger *et al* [9], amplification is expected as the Helmholtz number kr_0 is below 0.1, r_0 being the distance of a point dipole to the edge. This could occur in the present case at the BPF for a blade-tip force if $k_B \sqrt{d^2 + (h - R_t)^2} < 0.1$, thus for a tip-to-edge distance of about 1 cm at 6,000 rpm. Such a positioning is not likely to be encountered in practical applications; indeed it corresponds to a distance to the edge of 3.3% of wing chord, and 5% of propeller diameter. Yet the question of the effect of short distances

approaching the amplification regime is still open. Moreover, substantially lower frequencies would be produced by propellers of the same size but with lower blade numbers, making the issue more critical. For these reasons, a short distance of the order of the centimeter must be tested in the experiment.

Two regimes of interaction can be addressed with the present experimental setup, namely the true over-the-wing configuration, and an asymmetric pusher configuration. In the first case, ($h > R_t$, $d > 0$), significant masking by the wing is expected for observers located below the wing. In the second case, ($d < 0$), additional sound generation is expected from the operation of part of the blades through the wing wake when $h < R_t$ [10]. Finally, the searching domain has been determined in such a way that, for all configurations, the propellers and wing remain well within the core of the wind-tunnel jet, of nearly-uniform flow speed. It is limited by the green dotted line in Fig. 26. Preliminary numerical simulations have been performed to determine the nearly-uniform flow-speed area (see section 5.4.1).

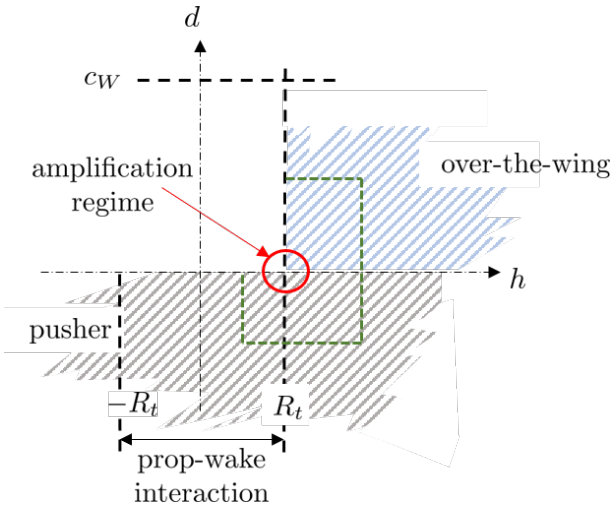


Figure 26: Domain of parameters h and d for the assessment of wing scattering. Indicative bounds of the searching domain as green dotted line.

5.3 Wind Tunnel Facility

Experiments are performed in the open-jet high-speed anechoic wind tunnel in the Fluid Mechanics and Acoustics Laboratory (LMFA) of *École Centrale de Lyon* (ECL) [11]. The nozzle dedicated to the project has an exit cross-section of 0.9 m height and 0.7 m width, with 'vignetted' corners. It issues in an anechoic chamber, as shown in Figure 27, with average length, height, and width of 10 m, 9 m, and 8 m, respectively. The chamber has slightly diverging walls made of fiberglass wedges coated by perforated metallic panels. An 800 kW electric motor drives the fan, which delivers the flow from an external environmental inlet to the outlet in the anechoic chamber, through an acoustically treated duct. Additionally, grid screens are installed before the final contraction of the duct, resulting in a residual turbulent intensity of less than 0.5%. The maximum design free-flow speed is of 60 m/s for the original rectangular outlet of 0.56 m height and 0.56 m width. The maximum achievable flow speed at the end of the present diverging nozzle, specially designed for the study, is about 30 m/s, due to the enlarged open test section.

5.4 Test Conditions

5.4.1 Numerical Simulations

Although the present investigation is not numerical, Reynolds-Averaged-Navier-Stokes (RANS) simulations were performed with the commercial ANSYS-FLUENT 2021 software, to determine the best-suited wing angle of attack for the experiment. Incompressible flow and steady-state were assumed. In addition,



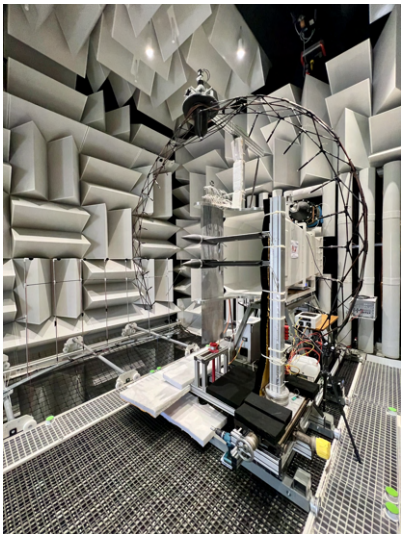


Figure 27: Overview of the empty anechoic room (left) and picture of the setup and nozzle (right).

the computational domain dimensions and boundary conditions were adjusted to the characteristics and location of the wind tunnel used for the experiments.

An appropriate mesh was created by discretizing the computational domain in an adequate number of elements. A grid independence study was carried out to ensure that the grid refinement does not affect the solution. This study gave the size of the grid elements with the lowest computational cost. The selected grid has 20×10^6 elements, the first layer of cells ensuring a maximum $Y^+ = 1$. Unstructured meshes with tetrahedral elements were created for the whole domain; however, structured meshes were used near the walls and the wing to capture the boundary layer effects. The Shear Stress Transport (SST) turbulence model was used alongside the turbulence model transport equations of turbulent kinetic energy κ and turbulent dissipation ω, due to its ability to model typical high-lift aerodynamic problems. It ensures the capture of transition effects at high turbulence levels and the calibration of the model coefficients for appropriate flow phenomena. A wide range of geometrical angles of attack was examined, from $\alpha = 0°$ to $= 12°$, selecting $\alpha = 10°$ for having a realistic lift coefficient.

5.4.2 Selected Reference Configuration

The selected wind tunnel speed for the experimental campaigns was 22 m/s, corresponding to a Reynolds number of 4.5×10^5, based on the chord length of the model wing. Tests were performed for different model configurations, varying the position of the propellers but maintaining propellers direction, and RPM settings. The incident flow was always aligned with the propeller axis. Prior to these tests, a reference configuration has been defined, as a clean configuration with no propellers. For this, the wing was also tested for a single deflection angle $\alpha = 10°$.

5.5 Instrumentation

5.5.1 Acoustic Measurements

Acoustic measurements were carried out with an array of 20 Bruel & Kjaer type 4958 1/4" free-field microphones, distributed around the model on a rotating arc antenna of 2 m diameter, as shown in Figure 28. The antenna rotates around the vertical axis to cover a portion of a sphere and obtain three-dimensional sound directivity patterns. The axis coincides with the trailing edge of the wing. The microphone data acquisition was performed through 4 synchronized AC/DC Coupling NI PXI-4472 boards of 8 analog inputs each, mounted in a NI PXI-1042Q chassis. The acquisition is controlled by a NI PXI-8331 interface module that gives PCs direct control of the PXIs-4472. A LabView environment

developed at the laboratory was also employed for the data acquisition at a 25.6 kHz sampling frequency. The data were acquired simultaneously for 30 s, providing power spectral densities (resolution 1 Hz).

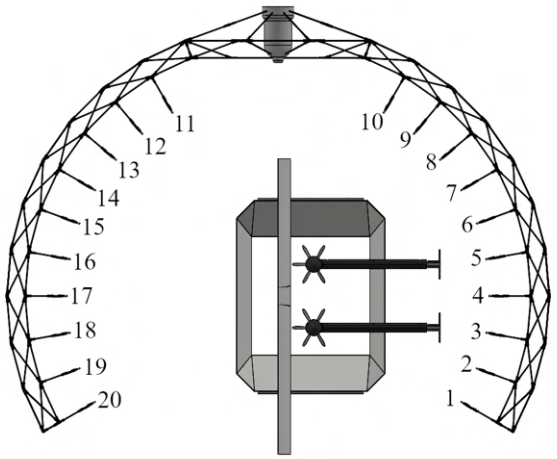


Figure 28: Antenna location regarding the wing-propellers system and microphone numbering. The antenna axis coincides with the wing trailing edge. Antenna set at 0° angle.

For practical reasons, the arc antenna of far-field microphones can be rotated around its axis by a maximum amount of ±45° with respect to a reference position perpendicular to the direction of the wind-tunnel stream. Larger angular displacements would make the measurements suffer from sound scattering by the lips of the nozzle and/or from contamination by the pseudo-sound pressure of the jet shear layers.

5.5.2 Static Pressure Measurements

The wing model instrumentation includes two chordwise sets of 32 steady-state pressure taps distributed on both pressure and suction sides, with refined distributions close to the LE and in the aft part on the suction side, where the propellers are positioned. In the reference state, the two rows of pressure taps are located in the center part of the vertical flow extent, at $50mm$ on each side from the mid-span. Arbitrary spanwise measuring positions can be reached by shifting the wing vertically with respect to the other parts of the setup. Indeed, distributed pressure-coefficient measurements are needed to characterize the aerodynamic performances of the wing in the presence of the propellers, some spanwise non-uniformity being expected. Figure 29 shows the positions of the pressure taps in the two instrumented cross-sections.

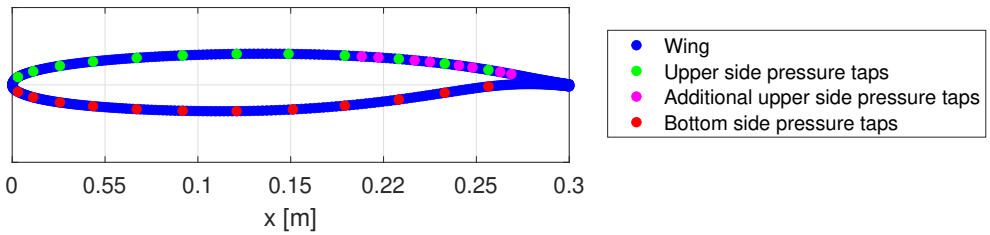


Figure 29: Pressure taps locations.

The pressure taps are connected to pressure tubes guided out of the wing and connected to a KMPS-1-64 Kulite® pressure scanner of 0.1% accuracy, which operates in a 1-2 psi range. The KMPS-1-64 pressure scanner module is designed for wind tunnels and accepts up to 64 pneumatic inputs. The module also incorporates a calibration valve that enables sensors to be automatically calibrated online and purges

the input lines of contaminants or condensation. Data are acquired for 20 seconds simultaneously for all pressure inputs via ethernet digital output, allowing integration into standard networks for connecting the Kulite ® pressure scanner to a local computer.

5.5.3 Aerodynamic Forces Measurements

The propeller torque moments, as well as tension and compression loads, were measured with a Futek MBA500 (100/100) Bi-Axial Load Cell. This torque/thrust sensor is temperature-compensated and able to achieve 0.2% nonlinearity and yet provide 125-150% over-capacity. Additionally, the voltage measurements from the strain gauge of the load cell are amplified through the Futek IAA100 amplifier, which allows for gains and filtering regulations. The data were acquired simultaneously for 30 s at a sample rate of 51.2 kHz.

5.6 Data availability

The data set for the B2-ECL configuration is publicly accessible on the Zenodo repository by using the following link: `https://doi.org/10.5281/zenodo.7925336`. The folders contain the corresponding README file for each set of results. Additionally, associated data includes the file ENODISE_experiments_matrix.xlsx which shows important information on the test matrix, for the interpretation of the measurements.

6 B3-VTOL

Configuration B3 concerns a conceptual flap-mounted propulsion system intended for vertical take-off. This configuration has been divided into two sub-configurations, B3-VTOL and B3-Flap. In this section, the baseline for configuration B3-VTOL is discussed. The study of this configuration is aimed at exploring the aerodynamic interactions which occur during ground proximity of multi-rotor configurations.

6.1 Wind Tunnel facility

The measurements for configuration B3-VTOL have been conducted in the High-Speed Laboratory (HSL) at the TU Delft. Since this configuration deals with the static testing of rotors, no wind tunnel is required. The measurements are therefore conducted in an enclosure of 2x3x2 m^3.

6.2 Propeller model

Two counter rotating rotors are installed with their axes perpendicular to a ground plane, see Figure 30. The two-blade twisted rotors comprise a radius of $R = 76.2$ mm, a pitch of 4 inches and a parabolic tip. The APC-brand rotors are commercially available and their model numbers are APC 6X4E and APC 6X4EP (identical but mirrored, for the counter-rotating configuration). Each rotor is driven by a geared in-runner brushless motor (type Hacker, B20 26 L kv2020 + 4:1).

6.3 Operating conditions

The rotors are operated at a shaft rotation speed of $\Omega = 167$ Hz. The rotors are not phase-controlled which means that the relative phase difference varies during acquisition. The discrepancy in rotational speed between the rotors is estimated to be equal to 0.25 Hz, resulting in a variation of the phase difference between the rotor blades, over the acquisition duration of the measurement. The Reynolds number, based on the sectional chord length at a nominal radius of $0.75R$, is $Re_c = 42{,}000$ and the tip Mach number is $M_{tip} = 0.22$. The rotors have a thrust coefficient of $C_t = 0.12$ and provide a thrust of $T = 2.14$ N. The rotors are operated in stagnant air representing a hover scenario (thus the advance ratio is $J = 0$), at conditions of normalised tip-to-tip rotor spacing $S/R = [0.05, 1.0, 2.0]$ and normalized height $H/R = [1.0, 2.0, 3.0, 4.0]$. Experimental conditions are summarized in Table 12.



Figure 30: Side-by-side rotor setup of configuration B3-VTOL.

Table 12: Two-rotor operating conditions

Rotor parameters and operation	
Rotation speed Ω [Hz]	167
Number of blades B	2
Radius R [mm]	76.2
Chord Reynolds Re_c	42,000
Tip Mach M_{tip}	0.22
Lateral separation S/R (tip-to-tip)	0.05-2
Height to ground H/R (disk-to-ground)	1-4
Thrust T [N]	2.14
C_t	0.12

6.4 Measurement Techniques

Two separate test campaigns have taken place. First of all, a characterization of the volumetric flow field has taken place using Lagrangian Particle Tracking. A second investigation focused on the unsteady flow behaviour using time-resolved Particle Image Velocimetry (TR-PIV) setup. Both measurement setups and processing techniques will be introduced here.

6.4.1 Lagrangian Particle Tracking

Volumetric velocity measurements cover the flow domain illustrated in Figure 31. Helium filled soap bubbles (HFSB) generated under controlled conditions [12] are employed that scatter sufficient light in conditions of volume illumination and imaging. Two HFSB generators are utilised producing each approximately 30,000 bubbles per second, with a mean diameter of 0.4 mm and nearly neutrally buoyant. The enclosure is seeded for two minutes prior to performing the measurement. The achieved seeding density is approximately 0.01 particles per pixel (*ppp*) corresponding to a spatial concentration of 0.5 particles/cm^3. The measurement volume is illuminated by a LaVision LED-Flashlight 300 device at a distance of 0.7 m below the measurement volume. Illumination is performed at a rate of 2.0 kHz and the duration of illumination for each pulse (pulse width) is $\delta t = 50$ µs. A tomographic imaging setup is composed of three high-speed CMOS cameras (Photron Fastcam SA1.1) placed outside the enclosure at a distance of 1 m from the measurement region. The cameras subtend a total angle of 38° (see Figure 31)

and are equipped with lenses of focal lengths $f = 60$ mm (camera 2) and $f = 50$ mm (cameras 1 and 3), set at numerical aperture $f_{\#} = 16$. The resulting measurement volume spans 20 x 31 x 33 cm^3 (4.3R x 4.0R x 2.6R). System synchronization is obtained with a LaVision Programmable Timing Unit (PTU 8) and each measurement comprises of 2000 recordings for a time duration of 1 s. The object-to-image mapping parameters are obtained with a calibration procedure based on a target recorded at 3 positions separated by 10 cm each. The residual calibration disparity is reduced to less than 0.1 pixels using the volume self-calibration method [13]. An overview of the measurement parameters is presented in Table 13.

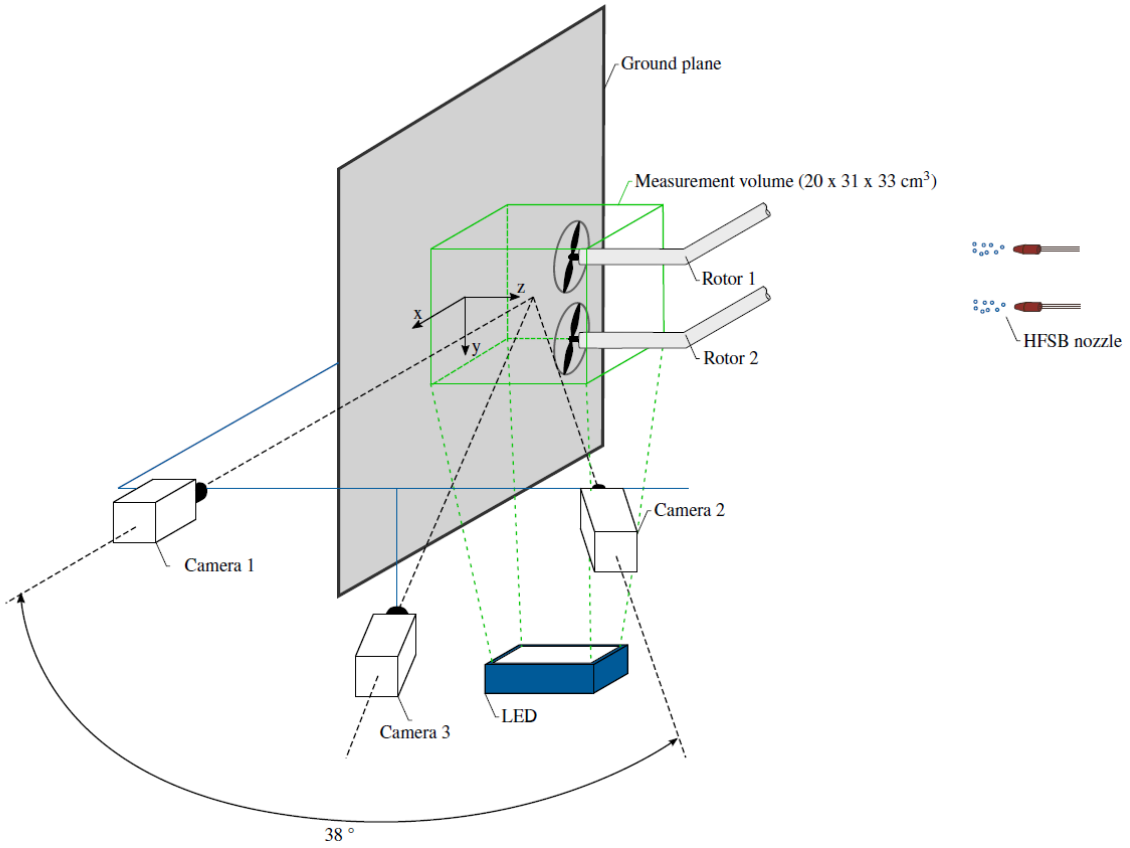


Figure 31: 3D schematic of the experimental apparatus, coordinate system and measurement volume for the 3D-PTV measurements.

Table 13: Lagrangian Particle Tracking illumination and imaging conditions

Measurement parameters	
f [mm]	1x 60, 2x 50
$f_{\#}$	16
Acquisition freq. [Hz]	2000
Sample time [s]	1
Pulse width [μs]	50
ppp	0.01
Field of View (Δx, Δy, Δz)	20x31x33cm^3

The raw footage from the cameras is first pre-processed using a high-pass frequency filter [14] that eliminates any stationary reflection from the ground plane and support struts of the rotors. As a second pre-processing step, the particle peak intensity is normalized and a Gaussian smoothing is applied.

The 3D particle motion analysis is performed with the "Shake-The-Box" algorithm [15]. The measurement delivers approximately 8000 particle tracks with a sampling frequency of 2.0 kHz. The maximum particle displacement within a particle track is approximately 20 pixels corresponding to a physical displacement of 6.4 mm.

Data reduction to a cartesian grid is performed for the time-averaged velocity fields. Time-average information is gathered in cubic bins of 20 mm size with a 75% overlap factor, yielding a spacing of the velocity vectors of 5 mm. Every bin comprises approximately 10,000 samples. However, the concentration varies across the measurement domain. Nevertheless, a minimum number of 100 samples is set as a criterion for a valid measurement.

The measurement uncertainty ϵ_u for the time-averaged flow field is statistically determined by the ratio between the relevant velocity fluctuations (axial velocity standard deviation) and the square root of the number of samples per bin. The measurement uncertainty ϵ_u was below 0.5% of the rotor-induced velocity in the majority of the domain, except for the shear layers along the boundary of the domain and close to the rotor blades, where it reaches up to $\epsilon_u = 1.5\%$.

6.4.2 TR-PIV

Planar PIV velocity measurements were acquired in the domain illustrated in Figure 32. During the measurements, Five HFSB generators delivered roughly 150,000 bubbles per second, which were nearly neutrally buoyant and had a mean diameter of 0.4 mm. The enclosure was seeded for two minutes prior to performing the measurement, and resulted in a density of roughly 0.01 particles per pixel (*ppp*) corresponding to a spatial concentration of 12 particles/cm^2. Laser illumination was provided by a Nd:Yag Continuum Mesa PIV 532-120-M laser. The laser beam was expanded by a cylindrical lens allowing a light sheet thickness of 2 cm. Its effective thickness was estimated using 3D flow data as 8 mm. Illumination was given with a pulse width of $\delta t = 150$ ns and a rate of 4.0 kHz.

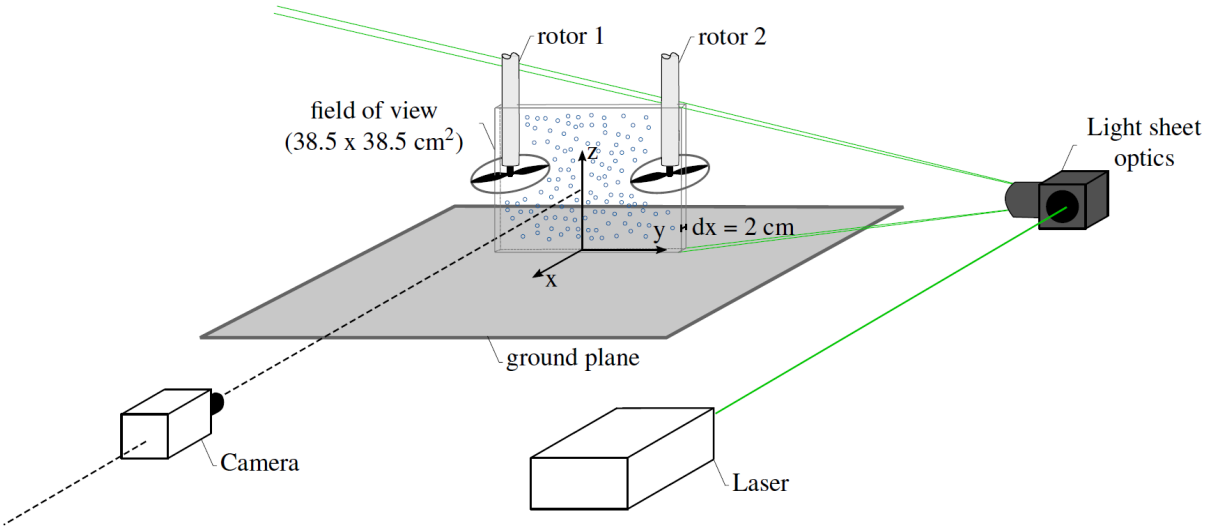


Figure 32: 3D schematic of the experimental apparatus, coordinate system and measurement volume for the 2D2C PIV measurements.

A high-speed CMOS camera (Photron *Fastcam* SA.5, 1024 × 1024 px^2) was used for imaging and placed outside the closed environment at a distance of 1 m from the measurement region. A lens with focal length $f = 50$ mm, and a numerical aperture set to $f_\# = 8$ captured a field of view of 38.5 × 38.5 cm^2 ($5R \times 5R$) at a magnification of $M = 0.053$. Synchronization between the cameras and the laser was obtained with a LaVision Programmable timing unit (PTU X). Each experimental run captured 2.7 s of data (approximately 11,000 recordings) and was repeated for six times, thus providing a total of

roughly 16 s (≈2750 rotor revolutions) for each of the two configurations. Measurement parameters are summarised in Table 14.

Table 14: TR-PIV illumination and imaging conditions.

Seeding type	HFSB
Seeding concentration (cm^{-2})	12
Illumination	Nd:Yag Laser
Sheet thickness dx (cm)	2
Pulse width δt (ns)	150
Repetition rate (Hz)	4000
Camera type	Photron *Fastcam* SA.5 (1024 x 1024 px^2)
Objective focal length f (mm)	50
Numerical Aperture $f_\#$	8
Optical Magnification M	0.053
Field of view (cm^2)	38.5 x 38.5
Seeding density ppp	0.01
Number of recordings	6 x 10917
Image analysis	Cross-correlation (24 x 24 px^2)

Two pre-processing steps were applied to the raw camera footage before computing PIV-based velocities. First, a minimum time filter was used to eliminate any stationary reflections from the ground plane and support struts of the rotors. Secondly, a sliding minimum filter with a length scale of 3 pixels was applied, to reduce any unsteady rotor blade reflections. Planar velocity components were inferred by cross-correlation between subsequent images, with a window size of 32×32 px^2 and an overlap of 75%. This resulted in a vector resolution of 8 mm and a vector spacing of 2 mm. The velocity field was then cropped to a physical domain of 31×27 cm^2. As a final post-processing step, time super sampling with a factor of 5 was applied.

The measurement uncertainty ϵ_w for the instantaneous velocity field has been computed using the method of correlation statistics as described by [16]. From this follows an average instantaneous uncertainty of approximately 4% of the rotor-induced velocity.

6.5 Data availability & naming conventions

The data sets for B3-VTOL are publicly accessible on the Zenodo repository by using the following link: `https://doi.org/10.5281/zenodo.7875780`. The B3-VTOL dataset consists of two folders. The folder "STB" contains the 4D-PTV particle tracks and the folder "TRPIV" contains the plane time-resolved measurements. The corresponding metadata and README files are also included within each folder.

7 B3-Flap

In this section, the baseline for configuration B3-Flap is discussed. The focus of the experimental campaign is on the trade-off between acoustic and aeropropuslive performance that can be achieved by varying the propeller position, and on the aerodynamic and propulsive loading related to the transition from vertical to forward flight conditions.

7.1 Wind Tunnel facility

The experiments for configuration B3-Flap were performed in the Aeroacoustic Wind Tunnel (AWT) facility at the Netherlands Aerospace Centre (NLR) in Marknesse, see Figure 33. The facility consists of an anechoic chamber (9 x 8 x 6 m), yielding an acoustic absorption rate of 99% above 200Hz. To increase the quality of the aerodynamic measurements, a closed test section was used, limiting the turbulence intensity to a maximum of 0.01% at a free-stream velocity of 20 m/s.

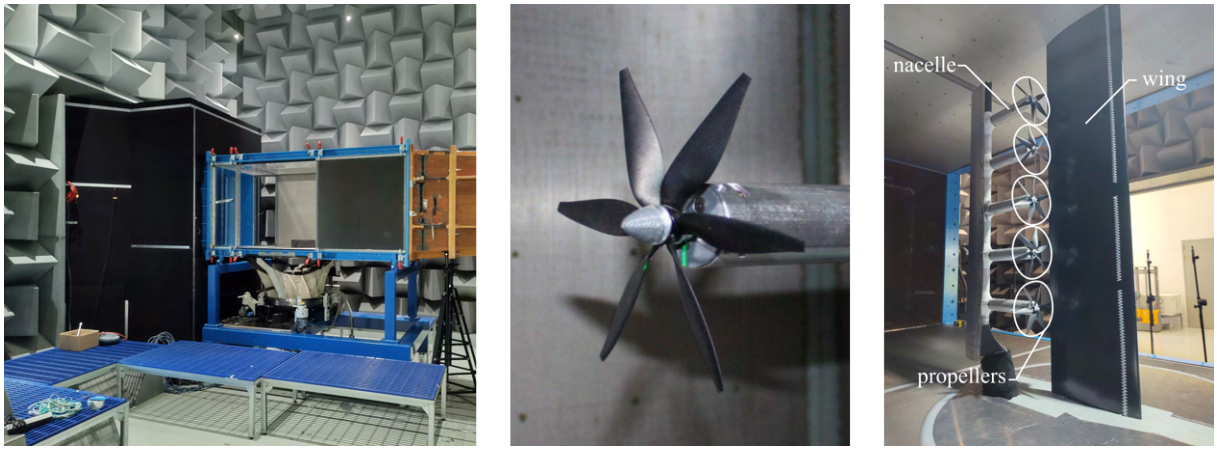


Figure 33: Side-by-side rotor setup of configuration B3-VTOL.

7.2 Propeller and wing model

A F15 wing model was mounted vertically on a turntable in the floor of the closed test section, as shown in the right image of Figure 33. The wing's chord comprises 240mm and the boundary layer was tripped at 10% chord on both the suction and pressure side. Over the suction side of the wing, a sting was connected to the same turntable as the wing. The sting serves as a support structure for five, span-wise distributed nacelles and aligns each nacelle's axis to the wing's chord direction.

Inside each nacelle, a brushless in-runner motor drives a custom design six-bladed propeller (radius of 63.5 mm) at a shaft frequency of 383 Hz. The blade design of this propeller is based on a benchmarked version for low-Reynolds application derived from a NACA4412 airfoil. For additional details on the blade design, the reader is directed to the work of Grande *et al.* [17]. The propeller has been manufactured with CNC out of aluminum with 0.02 mm precision, and cured to avoid material relaxation and oxidation.

7.3 Operating conditions

The experiments for B3-Flap have been split into three separate test campaigns, with an increasing degree of complexity of the model. First of all, the single isolated propeller is tested, then a single over-the-wing propeller, and finally five distributed propellers over-the-wing. The operating conditions will be discussed separately for each of these test campaigns.

7.3.1 Isolated propeller

The isolated propeller tests concern a fixed rotational speed and angle of attack. The free-stream velocity is varied to measure multiple advance ratios ranging from hover ($J = 0$) to cruise conditions ($J = 0.6$). The experimental conditions for the isolated propeller are summarized in Table 15.

Table 15: Operating conditions isolated propeller

rotational speed Ω (Hz)	383
free-stream velocity V_∞	[0, 7.3, 14.6, 21.9, 29.2, 36.5]
advance ratio J	[0, 0.15, 0.3, 0.45, 0.6, 0.75]
angle of attack α (°)	0
(3/4)R rotor blade chord Reynolds number Re_b	60,000
tip Mach number M_t	0.42

7.3.2 Single propeller over-the-wing

A wide range propeller advance ratios J and inflow angles α are investigated for the installed configuration. Furthermore, three different propeller positions along the wing's chord line are considered. The experimental conditions for the single over-the-wing propeller are summarized in Table 16.

Table 16: Operating conditions single OTW propeller

rotational speed Ω (Hz)	383
free-stream velocity V_∞	[0, 7.3, 14.6, 21.9, 29.2]
advance ratio J	[0, 0.15, 0.3, 0.45, 0.6]
angle of attack α (°)	[0, 2, 4, 6, 8, 10, 12, 14, 16]
rotor tip gap y/R	[0.17, 0.27]
rotor chordwise position x/c	[0.3, 0.6, 0.9]
rotor spanwise position z/R	$\pm$[0, 0.08, 0.16, 0.32, 0.48, 0.64, 0.8]
$(3/4)R$ rotor blade chord Reynolds number Re_b	60,000
wing chord Reynolds number Re_c	120,000 - 480,000
tip Mach number M_t	0.42

7.3.3 Distributed propellers over-the-wing

Finally, experiments are conducted on a setup similar to the single propeller, but now with 5 spanwise distributed propellers. The experimental conditions for the distributed over-the-wing propellers are summarized in Table 17.

Table 17: Operating conditions Distributed OTW propellers

rotational speed Ω (Hz)	383
free-stream velocity V_∞	[0, 14.6, 21.9, 29.2]
advance ratio J	[0, 0.3, 0.45, 0.6]
angle of attack α (°)	[-3, 0, 2, 4, 6, 8, 10, 11, 12, 13, 14, 15, 16, 20]
rotor tip gap y/R	0.27
rotor chordwise position x/c	[0.3, 0.6, 0.9]
rotor tip-to-tip separation z/R	0.05
$(3/4)R$ rotor blade chord Reynolds number Re_b	60,000
wing chord Reynolds number Re_c	240,000 - 480,000
tip Mach number M_t	0.42

7.4 Measurement Techniques

A wide range of measurement techniques are conducted which will be discussed separately.

7.4.1 Integral loading

For the center nacelle (i.e. the mounting of the center propeller), the brushless motor is connected to the nacelle using two parallel-mounted uni-axial FUTEK LSB205 load cells and a FUTEK QTA141, which allows for thrust and torque measurements on the propeller. The load cells are excited with 7 volts of direct current (VDC) by a single power supply. Repeated measurements showed a maximum deviation of 2% for thrust and 5% for torque.

The integral loading of the wing is measured by a custom-made six-component force balance. In the lift and drag direction, the balance has a capacity of 1800 N and 325 N, respectively. The uncertainty as a percentage of the full load range is 0.13 % for the lift direction and 0.8 % for the drag direction.

7.4.2 Acoustics

Acoustic measurements were performed to both measure the increase in noise of the propeller and to quantify the effect of noise shielding. The noise of the propeller is measured using a microphone array consisting of 64 microphones, see Figure 34. The array is positioned outside the test section at a distance of 0.70 m and angled towards the suction side of the wing. Additionally, three free-field microphones are positioned outside the test section on the pressure side of the wing to investigate the potential of noise shielding by the wing. The free-field microphones are positioned at a distance of 2 m from the center of the test section. All microphones are sampled at a frequency of 41 kHz for a time duration of 20 s for each data point.

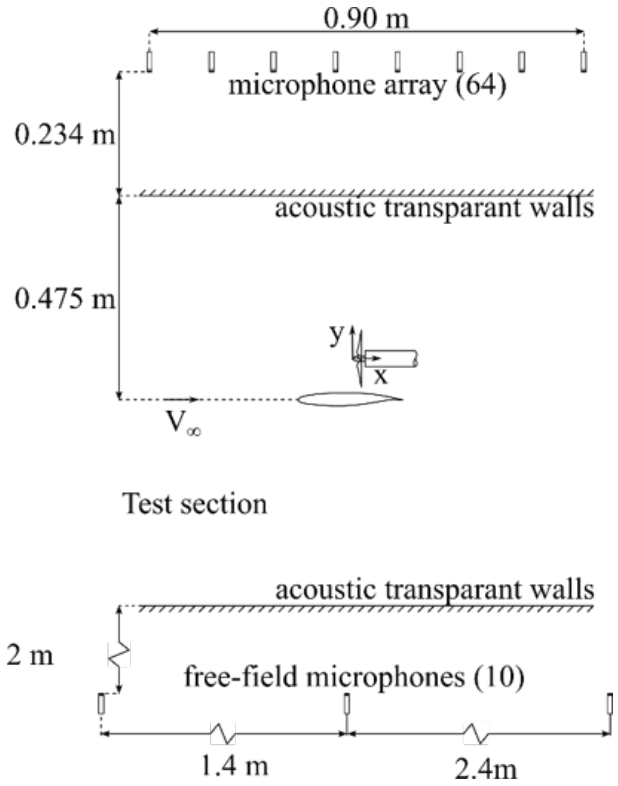


Figure 34: Microphone arrangement in AWT for configuration B3-Flap.

7.4.3 Pressure orifices

In the center span position of the wing, 59 static pressure taps are fitted. The location of the center span pressure taps along with the contour of the wing profile is presented in Figure 35. Two additional, coarser spaced, pressure tap rows are positioned at 25%- and 75%-span to evaluate the two-dimensionality of the flow. All pressure measurements are averaged over 20 s. For a number of data points, the propeller is traversed along z-direction, in steps of 10 mm to a maximum displacement of 50 mm (0.8 R) in both positive and negative z-direction. This allows for a surface pressure reconstruction to investigate spanwise variations.

7.4.4 Stereoscopic Particle Image Velocimetry

The flow at the inflow of the single over-the-wing propeller is characterized using stereoscopic particle image velocimetry (sPIV). The flow is seeded with DEHS tracer particles ($\tau = 2\ \mu$s) which are illuminated by an evergreen laser (200 mJ/pulse) in a sheet of 3mm thickness. Illumination is performed at a rate

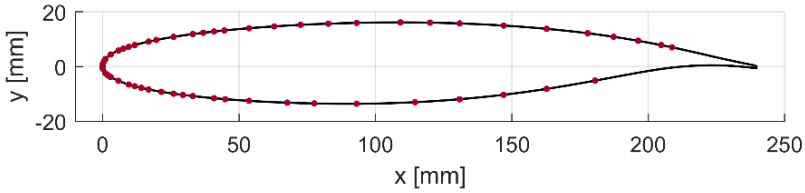


Figure 35: Pressure tap positions in F15 wing model.

of 15 Hz and the duration for each pulse (pulse width) is δt = 25 ns. Recording is performed by two sCMOS cameras (Imager sCMOS CLHS) placed outside the section at a distance of 0.6 m from the center of the measurement region. The camera is equipped with an objective of focal length f = 50 mm, set at numerical aperture f# = 8. The resulting field of view spans 19 x 25 cm^2 (3 R x 4 R). System synchronization is obtained with a LaVision Programmable timing unit (PTU X) and each measurement comprises at least 300 recordings for a time duration of 20 s. An overview of the illumination and imaging conditions is presented in Table 3.

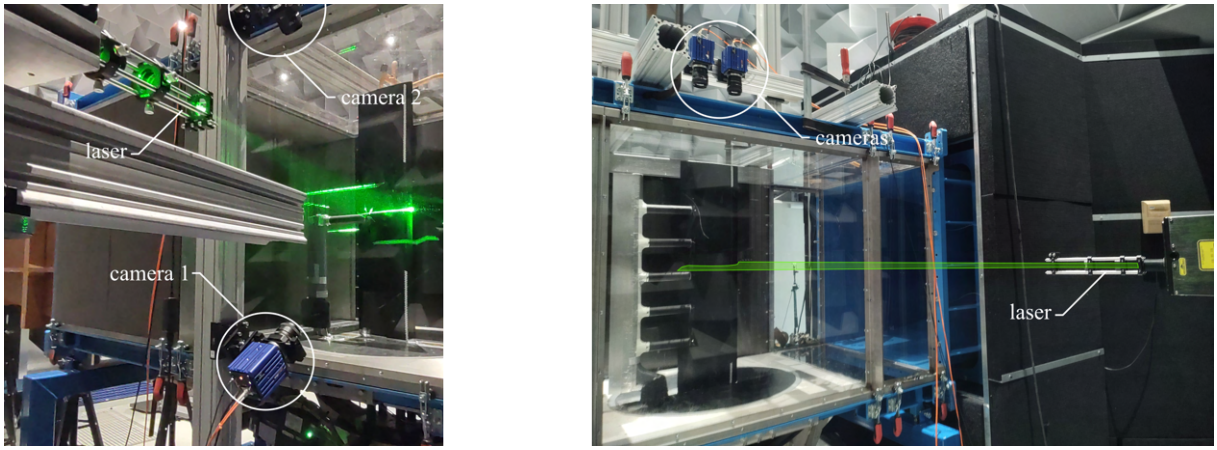


Figure 36: Stereoscopic PIV setup (left) and 2D2C PIV setup (right) used for the aerodynamic investigation of B3-FLap.

7.4.5 2C Particle Image Velocimetry

For the 5 spanwise distributed propeller, 2D2C PIV is employed over the complete suction side of the wing. The setup uses similar hardware and settings as the sPIV setup, with a resulting field of view of 36 x 24 cm^2 (6 R x 4 R). Each measurement comprises of 200 recordings for a time duration of 13 s.

7.5 Data availability & naming conventions

The data sets for B3-Flap are publicly accessible on the Zenodo repository by using the following link: `https://doi.org/10.5281/zenodo.8283630`. The B3-FLAP contains four folders: "CAD", "IsoPropeller", "SinglePropeller" and "Distributed propeller". The "CAD" folder contains the propeller airfoil sections and CAD files while the other three folders contain measurements of the three test campaigns for B3-FLAP. Each measurement folder has a sub-folder containing either the acoustic, pressure, loading or velocimetry data. The corresponding metadata and README files are included within each of these sub-folders.

8 C - VKI

8.1 Description of the ALCOVES anechoic test room

The experimental campaign is carried out in the ALCOVES anechoic laboratory at the von Karman Institute for Fluid Dynamics, Belgium.

The room has a cut-off frequency of 200 Hz, and an auxiliary fan is used to drive the flow in the wind tunnels. The noise propagation of the auxiliary fan is prevented through the use of acoustic treatments in the pipe that drives the flow. Furthermore, desired requirements for good quality measurements are:

- minimized acoustic background noise
- clean flow quality
- reduced effects of wake re-circulation

The configuration of the ALCOVES laboratory adapted for the experimental campaign is shown in Figure 37.

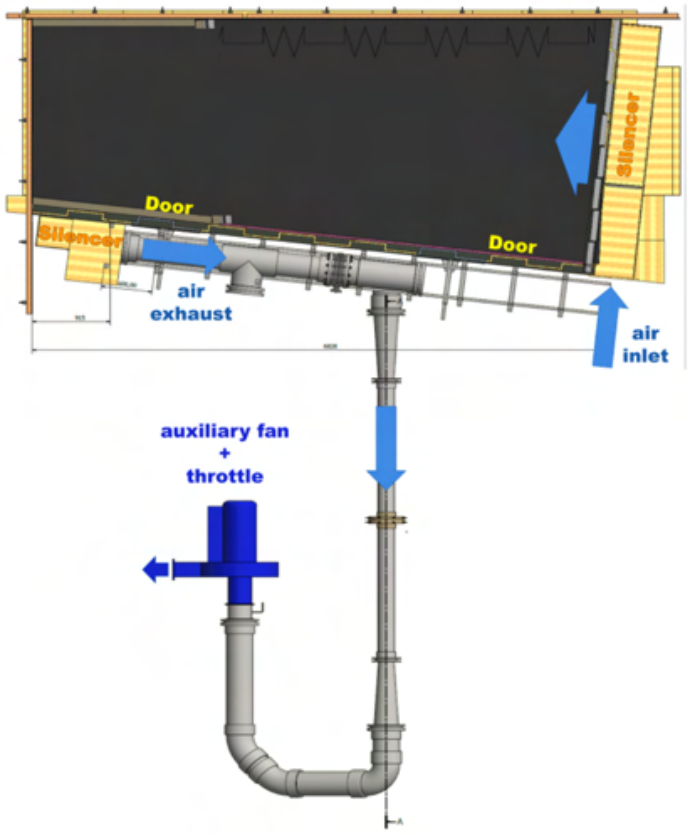


Figure 37: Alcoves facility scheme.

8.1.1 Design of the coaxial rotors system and instrumentation structure

The multi-rotor propulsion system has been designed, manufactured and assembled at VKI for testing and evaluating the aerodynamic performance and acoustic signature of coaxial contra- and co-rotating rotors. The sketch of the setup and the dimensions are illustrated in Figure 38.

The test setup is composed of two independent propulsive systems. The two test stands are placed behind each other and aligned on the same axis to minimize aerodynamic interactions and reduce acoustic

scattering. The stand placed at the rear is designed with a long shaft supported with several bearings and passes through the first stand. The axial spacing between the front and rear propellers varies in a range of [2, 4] cm by moving the front propeller on the long shaft. The front stand is composed of the same elements but the shaft had to be hollow in order to accommodate the long shaft from the rear stand. Furthermore, the long shaft aligns and holds together the rotor and the stator of the front motor. The hollow shaft is also aligned with means of bearings placed between it and the long shaft. Moreover, the presence of the two test stands allows independent change of the RPM and sense of rotation of the two propellers. Hence, both co- and contra-rotating configurations are analyzed. During the experimental campaign, the test stands are shielded by a fairing (see Figure 40).

The experimental tests will be carried out using 2- and 3-blade Mejzlik propellers 13"x4.2 model.

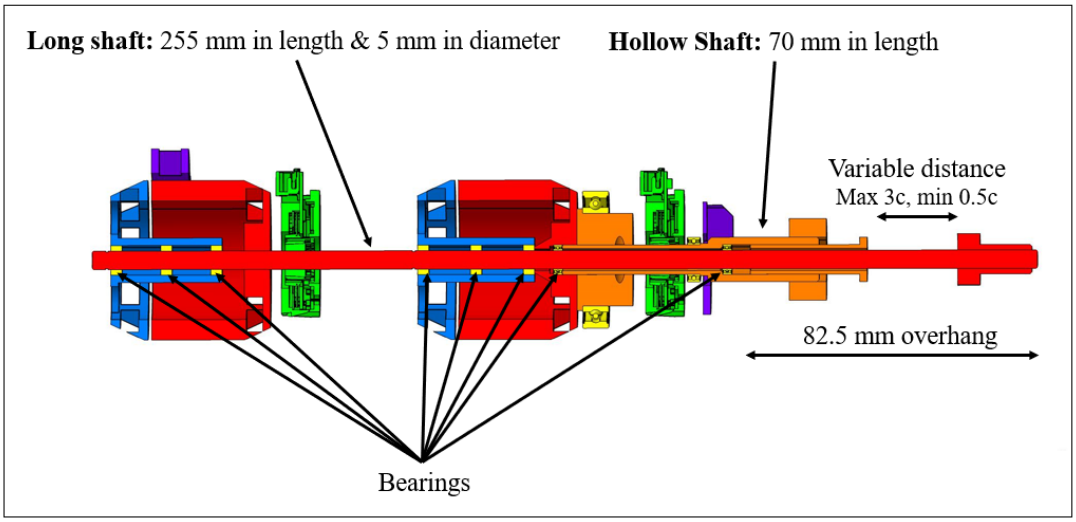


Figure 38: Scheme of multi-rotor setup.

To limit the overheating of the motors and operate at a temperature inferior to 36°C, the setup includes an active cooling system, in addition to the passive cooling coming from air movement generated by means of the motors and the cold air flow generated by the propellers. The cooling system is connected to a cold inflow of air, that comes from a pressure line in the ALCOVES facility and envelopes the instrumentation within it (see figure 39). Motors 1 and 2 along with the load-cell implement each a thermo-couple, recording their respective temperature.

The picture of the setup is shown in Figure 40.

The test stands are mounted on a supporting structure (see Figure 40) designed to guarantee high stabilization along the vertical and horizontal axis. Hence, vibration-damping elements are mounted on the structure. The structure was mainly designed and manufactured to be installed at the back of the setup in order to minimize noise-scattering effects. The structure is covered by acoustic foam during the experimental tests.

Both test stands are equipped with the necessary sensors to measure the aerodynamic performance of the system, shown in Figure 41. More specifically, the rotational speed is measured by means of two tachometers which are two reflective sensors (VISHAY TCRT500). The latter is composed of an infrared emitter and a phototransistor. By placing a reflective surface on the respective shafts, we can measure the frequency at which they are rotating, hence their RPM. The propellers' phase angle is detected by two encoders CUI Devices AMT 22 type. The encoders ensure an accuracy of 0.2° up to 8000 RPM, and they allow control and vary the phase between the front and rear propellers while co-rotating at the same RPM.

The selected motors are T-Motors AT2814 Long Shaft, typical of small UAV applications. Their maximum range of rotation is 10000 RPM, exploiting 70% of the motor power. The motors are controlled using Scorpion Tribunus II 12-80A ESC SBEC controllers.

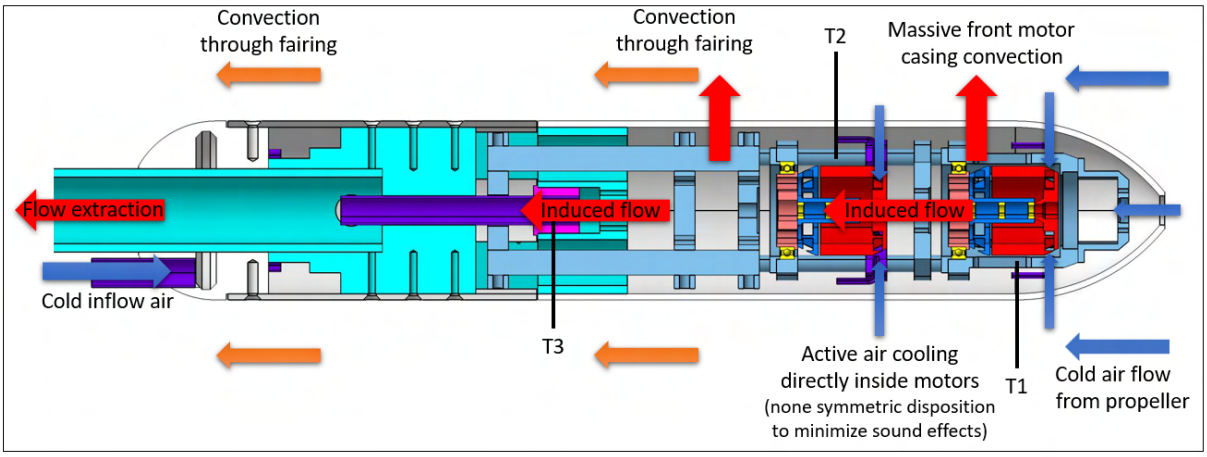


Figure 39: Active and passive cooling system.

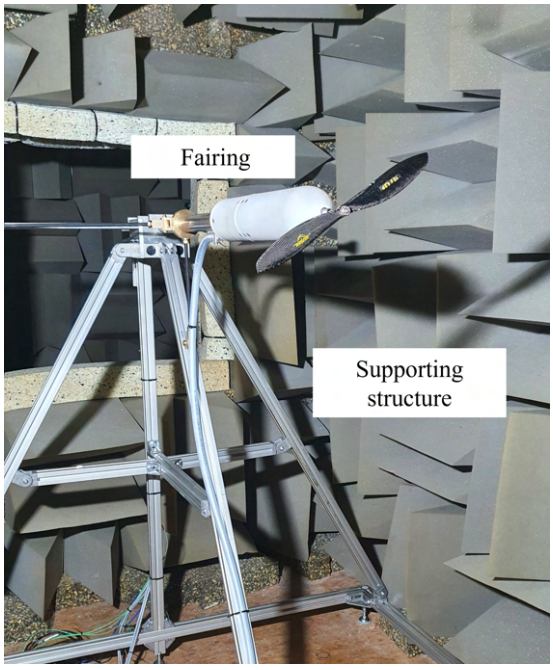
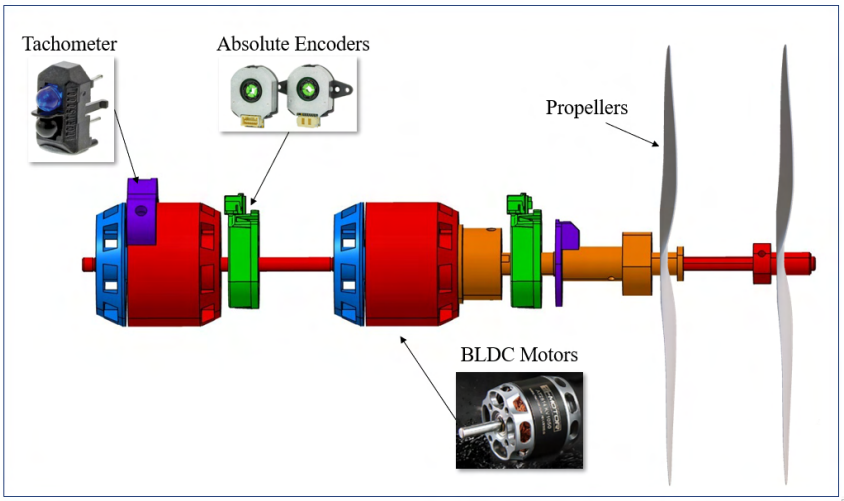


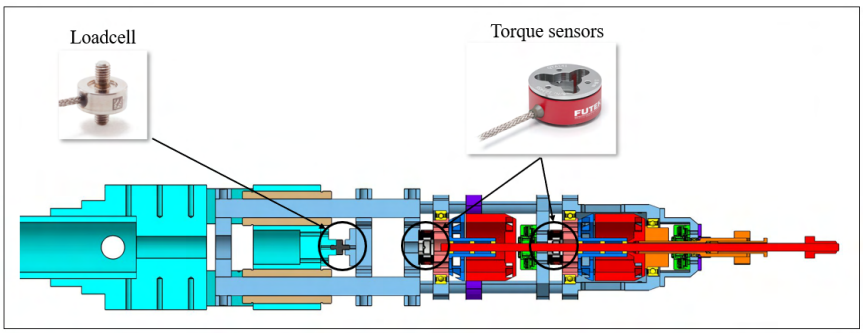
Figure 40: View of the setup adapted in the ALCOVES facility.

Furthermore, the overall thrust of the system is measured employing a single Futek LCM100 (FSH03828) loadcell that is placed between the rigid structure of the setup and the free two test stands that are guided with two low friction balls sleeves, shown in Figure 41(b). In order to minimize the impact of induced drag created by the fairing, the fairing is completely decoupled from the load cell.

Finally, the torque is measured by Futek QTA141 (QSH01827) sensors. The latter are hollow reaction torque sensors that are attached between a rigid part of the setup and the stator of each motor and are supported by means of low-friction bearings to minimize extraneous loads.



(a)



(b)

Figure 41: Schematic of sensor measurements setup.

8.1.2 Acoustic

The acoustic measurements were performed by means of three G.R.A.S. 40PL microphones, as shown in Figure 42.

The position of the microphones is referred to the center of a Cartesian coordinate system with origin in the center of the rear propeller, specifically *Propeller* 2, disk. Here, the z-axis was oriented positively along the rotor axis, pointing upstream. The y-axis represented the downstream direction along the middle of the disk, and the x-axis completed the system based on right-hand rule.

Mic 0 was positioned in the $x-z$ plane, aligned along the negative x-axis, and located at a distance of 65 cm. Mic 1 was situated upstream of the rotor, inclined at 10.6°, and positioned 56 cm away from the rotor axis. Furthermore, Mic 2 was placed along the negative y-axis, with a distance of 83 cm. The above-mentioned configuration is reported in Figures 43(a)-43(b). The data acquisition system consisted

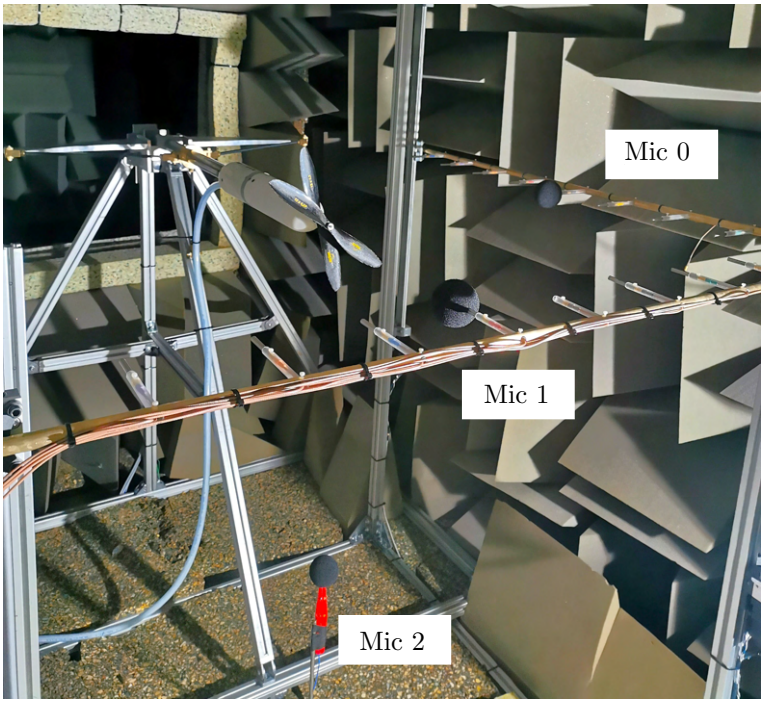


Figure 42: Microphone setup in ALCOVES - VKI.

of a cDAQ-9178 chassis equipped with a NI-9234 module. The raw signals have been acquired by means of LabView GRAS MIC Main v1.4 software over a time acquisition of 30 sec. A piston phone type 4231 B&K was used to convert the GRAS-type microphone's Voltage acquisition to pressure units Pascal using an acoustic wave emitted at a frequency of 1 KHz corresponding to 94 dB. The sensitivities of Mic 0, 1 and 2 were found to be $18.2885 * 10^{-3}$, $13.7234 * 10^{-3}$ and $13.2797 * 10^{-3}$ [V/Pa] respectively.

The Sound Pressure Level (SPL) (dB) is estimated as follows:

$$SPL = 10 \log_{10} \frac{PSD\Delta f}{p_{\text{ref}}^2}, \tag{1}$$

where the PSD [dB/Hz] indicates the Power Spectral Density of the signal, Δf [Hz] is the frequency resolution of the signal, and $p_{\text{ref}} = 20 \cdot 10^{-6}$ [Pa] is the reference pressure. The PSD was computed by means of Welch's method using the following parameters:

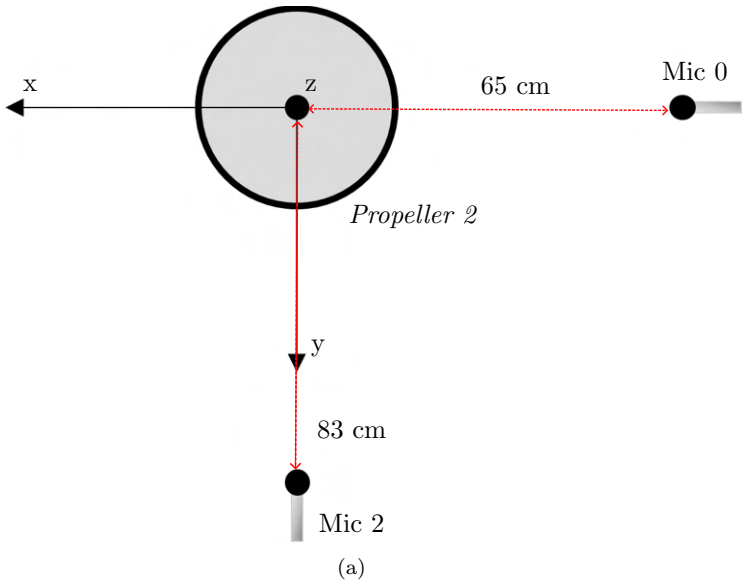
- Sampling frequency f_s 51 200 Hz,
- Hanning window with 2^{13} number of segments,
- 2^{12} number of points to overlap between segments,
- and 2^{14} length of FFT.

8.1.3 Content of the dataset

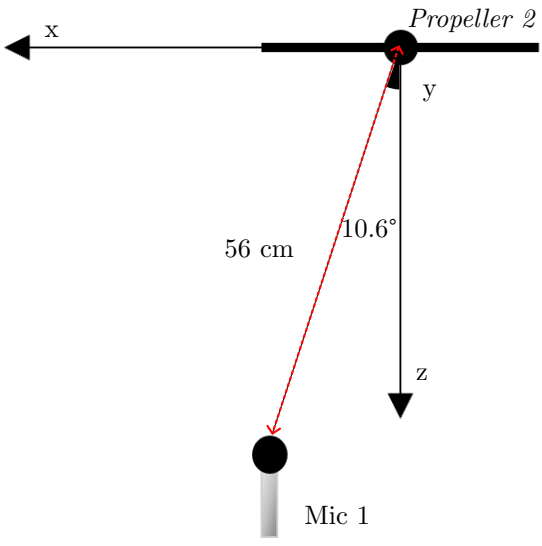
An experimental dataset for the aerodynamic and acoustics characterization of single and coaxial Mejzlik 2-blades propellers has been recorded and published on the open-source ZENODO platform [18].

Sound Pressure Level measurements

All the acoustic measurements are in the folder *SPL*. The latter comprises two subfolders for each *Configuration* investigated, Contra_Rotating_Rotor and Single_Rotor. The former refers to the



(a)



(b)

Figure 43: Microphone setup in ALCOVES

front/upstream rotor rotating clockwise and the aft/downstream rotating counterclockwise (seeing the system from the upstream side). The latter refers to the single propeller placed on the hollow shaft (Propeller 2 in 41(a)). The *Contra_Rotating_Rotor* folder comprises subfolders named d_*d*_cm, where *d* indicates the variable spacing between front and rear propellers. The distance *d* is in the range of 2 and 4 cm, specifically *d* has values of 2, 2.5, 3, 3.5 and 4 cm.
The folders *Single_Rotor* and d_*d*_cm include 3 subfolders named Mic_*y*, with *y* the index of the microphones: 0, 1 and 2. The acoustic measurements and the list of test cases are stored in the Mic_*y* folders and reported in SPL_$Configuration_d$cm_mic_*y*.*txt* and Test_Case_$Configuration_d$cm_mic$_y$.*csv* files respectively.
The former is a *n* x 8193 2D array, with *n* the number of the specific test case in string format reported

in Test_Case_$Configuration$_dcm_mic$_y$.csv (of n x 1 dimensions), and 8193 the length of the SPL array. More specifically, the name convention used in the Test_Case_$Configuration$_dcm_Mic$_y$.csv files is SPL_$System$_mic_y_d_cm_rpm_RPM with $System$ is Contra_Rotating for contra-rotating propellers and Propeller_2 for the single propeller. The rpm indicates the rpm [2pi/60 rad/s] used in the tests: 4000, 4100, etc.
The noise emitted by both *Motor 1* and *Motor 2* (of *Propeller 2* and *Propeller 1* respectively) has been recorded for 4000, 5000, 6000 and 7000, and stored in the subfolder *Motor_1_Motor_2* of *Contra_Rotating_Rotor* folder. The data are reported for each Mic_y, along with $test_case_Motor_1_and_Motor_2_mic_y.csv$ files.
The Frequency_$Configuration$.txt are 8193 x 1 array and are stored in the respective $Configuration$ subfolders.
Eventually, the SPL folder comprises a subfolder named *Cooling*, where the noise emitted by the cooling system alone has been reported for the three microphones.

Torque measurements

In the folder $Torque$ the mean values of aerodynamic torque and the respective rpm of the specific test cases are stored in *.txt* format. The convention used for naming the data files is Torque_$Motor_Configuration_d$_cm, with $Motor$ as m1 and m2 indicating Motor 1 and Motor 2, $Configuration$ and d defined as in Section 8.1.3. The torque [Nm] has been acquired over a time acquisition of 30 s at a rate of 10 Hz, and only the mean values have been reported in this database.
The Torque_$Motor_Configuration_d$_cm.txt file is a n x 2 matrix, with n the number of values of RPM = Revolutions per minute [2pi/60 rad/s] (e.g. 4000, 4100 ...), and the second column to the torque mean value.

9 Conclusions

A number of experimental campaigns have been successfully conducted on a wide variety of configurations as defined in the Enodise proposal. Each of these experiments and the accessible data has been described in this deliverable. The experimental data, including CAD geometry, is available for open access in the Zenodo repository.

References

[1] Leandro D. de Santana, Martinus P. Sanders, Cornelis H. Venner, and Harry W. Hoeijmakers. The utwente aeroacoustic wind tunnel upgrade. pages 1–12, 2018. Description of the upgraded acoustic wind tunnel in the University of twente (currently the open flow is working).

[2] Fernanda L dos Santos, Laura Botero-Bolívar, Cornelis H Venner, and Leandro D de Santana. Analysis of the remote microphone probe technique for the determination of turbulence quantities. *Applied Acoustics*, 208:109387, 2023.

[3] Yannick D. Mayer, Hasan Kamliya Jawahar, Máté Szőke, Syamir Alihan Showkat Ali, and Mahdi Azarpeyvand. Design and performance of an aeroacoustic wind tunnel facility at the university of bristol. *Applied Acoustics*, 155:358–370, 2019.

[4] S.A. Showkat Ali, M. Azarpeyvand, and C.R. Ilario da Silva. Trailing-edge flow and noise control using porous treatments. *Journal of Fluid Mechanics*, 850:83–119, 2018.

[5] S.A. Showkat Ali, M. Azarpeyvand, M. Szőke, and C.R. Ilario da Silva. Boundary layer flow interaction with a permeable wall. *Physics of Fluids*, 30(8):085111, 2018.

[6] Jochen Wild. Mach and reynolds number dependencies of the stall behavior of high-lift wing-sections. *Journal of Aircraft*, 50(4):1202–1216, 2013.

[7] Nando van Arnhem, Reynard de Vries, Tomas Sinnige, Roelof Vos, Georg Eitelberg, and Leo LM Veldhuis. Engineering method to estimate the blade loading of propellers in nonuniform flow. *AIAA Journal*, 58(12):5332–5346, 2020.

[8] Reynard de Vries, Nando van Arnhem, Tomas Sinnige, Roelof Vos, and Leo L.M. Veldhuis. Aerodynamic interaction between propellers of a distributed-propulsion system in forward flight. *Aerospace Science and Technology*, 118:107009, 11 2021.

[9] Michel Roger, Stéphane Moreau, and Korcan Kucukcoskun. On sound scattering by rigid edges and wedges in a flow, with applications to high-lift device aeroacoustics. *Journal of Sound and Vibration*, 362:252–275, 2016.

[10] M. Roger, D. Acevedo Giraldo, and M. Jacob. Acoustic versus aerodynamic installation effects on a generic propeller-driven flying architecture. *Int. J. of Aeroacoustics*, 2022.

[11] M. Sunyach, B. Bruiel, and G. Comte-Bellot. Performance of the high speed anechoic wind tunnel at lyon university. *NASA Technical Report*, 1986.

[12] D.E. Faleiros, M. Tuinstra, A. Sciacchitano, and F. Scarano. Generation and control of helium-filled soap bubbles for piv. *Experiments in Fluids*, 60:1–17, 2019.

[13] B Wieneke. Volume self-calibration for 3d particle image velocimetry. *Experiments in fluids*, 45(4):549–556, 2008.

[14] A. Sciacchitano and F. Scarano. Elimination of piv light reflections via a temporal high pass filter. *Measurement Science and Technology*, 25(8):084009, 2014.

[15] D. Schanz, S. Gesemann, and A. Schröder. Shake-the-box: Lagrangian particle tracking at high particle image densities. *Experiments in fluids*, 57:1–27, 2016.

[16] B. Wieneke. Piv uncertainty quantification from correlation statistics. *Measurement Science and Technology*, 26(7):074002, 2015.

[17] E Grande, G. Romani, D. Ragni, F. Avallone, and D. Casalino. Aeroacoustic investigation of a propeller operating at low reynolds numbers. *AIAA Journal*, 60(2):860–871, 2022.

[18] Erica Gallo, Julien de Decker, Pauline Haezebrouck, Alessandro Zarri, and Christophe Schram. H2020 enodise: Experimental dataset of configuration c vki, doi:10.5281/zenodo.8334930, May 2023.